Iron addition for long-term phosphate fixation

Sébastien Fauqué

Deltares
Enabling Delta Life

Utrecht University

Iron addition for long-term phosphate fixation

By

Sébastien Fauqué

In partial fulfillment of the requirements for the degree of Master of Science

in Marine Sciences at Utrecht University

May 2019

Utrecht, the Netherlands

Contact	safauque@gmail.com	
Supervisors	Dr. Leonard Osté	Deltares
	Dr. Thilo Behrends	Utrecht University

Deltares
Enabling Delta Life

Utrecht University

Preface

This thesis completes the requirements for the degree of MSc in Marine Sciences from the Faculty of Geosciences at Utrecht University, the Netherlands. This research was made possible with the help of Dr. Leonard Osté (Deltares) and Dr. Thilo Behrends (Utrecht University). I would like to thank Leonard Osté, Thilo Behrends, and Gerlinde Roskam for their supervision, fieldwork help, and patience during every chapter of this project. I would like to thank Reinier Groeneveld for his help during core slicing and fieldwork. Additionally, I would like to thank Dr. Wilko Verweij for his help with troubleshooting.

Furthermore, I would like to thank my family for their support during my education. Finally I would like to thank my Utrecht friends for making this degree an enjoyable experience.

Abstract

Eutrophic conditions due to high phosphate loading represents a significant water quality issue in the current and coming decade. Iron has therefore been suggested as a solution to bind phosphate despite its redox sensitivity. Iron's redox sensitivity causes Fe based P fixation to occur through two different processes in oxic sediments and anoxic sediments. In oxic sediment $Fe(III)_{(s)}$ adsorbs $PO_4^{3-}{}_{(aq)}$ to its surface where under suboxic conditions, Fe(III) will be reduced to Fe(II) and releasing $PO_4^{3-}{}_{(aq)}$. Vertical upwards $Fe(II)_{(aq)}$ transport and lead to Fe oxidation and ferrous wheel functioning while downwards transport to anoxic zones may lead to authigenic vivianite mineralization under favorable conditions. Conditions unfavorable to ferrous wheel functioning and vivianite mineralization are known to be affected by $SO_4^{2-}{}_{(aq)}$ and OM but the long-term understanding of shallow lake P fixation as a result of iron addition is lacking.

Here the porewaters and sediments of 4 iron treated shallow lakes and 3 untreated shallow reference lakes have been investigated. Surface and porewater analyses were carried out through spectrophotometric measurements, ICP-OES, and IC from which saturation indices were calculated. Sediments were analyzed through CN, CS, TGA, and XRF-P. Quantification of treatment iron was investigated as an issue related to treatment duration and viability. Results reveal $Fe_{(s)}$ recovery that is at least 87% and increased $P_{(s)}$ and $S_{(s)}$ retention compared to reference lakes. Controls on recovery are suggested to be related to treatment method iron application heterogeneity and groundwater fluxes.

Redox zonation in treated lakes has been affected by iron addition. Elevated $Fe(II)_{(aq)}$ concentrations at deeper depths have indicated that iron reduction is occurring over a larger depth interval. This has resulted in the simultaneous removal of $Fe(II)_{(aq)}$ and $SO_4^{2-}{}_{(aq)}$ with depth. This indicates an effect on iron redox cycling and conditions for authigenic vivianite mineralization. By affecting the redox zonation $Fe(II)_{(aq)}$ may be hindered from diffusing upwards by FeS_x mineralization in the presence of $S^{2-}{}_{(aq)}$ limiting iron within the ferrous wheel. Additionally, authigenic vivianite mineralization may be favored if reactive Fe(III) is reduced in the absence of $S^{2-}{}_{(aq)}$. Sampled lakes indicate several favorable sediment and porewater layers where authigenic vivianite may be formed and ferrous wheel function is occuring. This suggests that iron addition can be an effective method of long-term phosphate fixation.

Table of Contents

Table of Abbreviations

SWI = sediment water interface

Waters = surface and pore waters

SI = saturation index(ces)

OM = Organic matter

$Fe(II)_{(aq)}$ = surface and porewater Fe^{2+} (in aqueous, nanoparticulate, or <0.20 µm colloidal phase)

$Fe(III)_{(aq)}$ = surface and porewater Fe^{3+} (in aqueous, nanoparticulate, or <0.20 µm colloidal phase)

$Fe_{(s)}$ = solid phase iron in the sediment layer

$PO_4^{3-}{}_{(aq)}$ = aqueous phosphate in water (in aqueous, nanoparticulate, or <0.20 µm colloidal phase)

$SO_4^{2-}{}_{(aq)}$ = aqueous sulphate in water (in aqueous, nanoparticulate, or <0.20 µm colloidal phase)

$S_{(s)}$ = solid phase sulfur in the sediments

$S^{2-}{}_{(aq)}$ = aqueous sulfide in water

$Fe_{(aq)}/PO_4^{3-}{}_{(aq)}$ = aqueous total iron/ aqueous phosphate ratio

$Fe_{(s)}/P_{(s)}$ = solid phase total iron/total phosphorus ratio in sediments

$P_{(s)}/Fe_{(s)}$ = solid phase total phosphorus/total iron ratio in sediments

$Fe_{(s)}/S_{(s)}$ = solid phase total iron/total sulfur ratio in sediments

$S_{(s)}/Fe_{(s)}$ = solid phase total sulfur/total iron ratio in sediments

1. Introduction

A consensus of several global limnologists has described eutrophication as the leading problem facing fresh waters of the present and coming decade (Downing, 2014). Anthropogenic eutrophication is the process of humans overly enriching a water body with growth limiting nutrients ultimately leading to extreme plant and/or algae growth (Schindler, 2006). This increased algal growth has had significant impacts on oxygen availability, biogeochemical cycles, and internal nutrient cycling (Hutchinson, 1957; Hall & Smol, 1999; Hupfer & Lewandowski, 2008).

Since the development of artificial fertilizers and the subsequent agricultural boom, enrichment of phosphorus (P) and nitrogen (N) in soils has led to rapid nutrient increases in aquatic systems through overland and groundwater transport during rainfall events (Smith et al., 1999; Ekholm and Lehtoranta., 2012). The subsequent eutrophic conditions represent a reduction of the limiting factors controlling algal populations (Schindler, 2012) and harmful effects including oxygen depletion, biodiversity loss, poor water clarity, and toxic algal blooms which ultimately lead to reduce benefit of the ecosystem (Figure 1) (Hutchinson, 1957; Carpenter et al., 1998). Eutrophic damage poses economic stressors on the fishing, tourism, and healthcare industries which drives scientists, water managers, and policy makers to explore remediation solutions (Dodds et al., 2008). This has led to the development of several worldwide legislative projects and they aimed at increasing ecological water quality. Since the 1970s freshwater restoration procedure in highly developed countries favored P control from external point sources such as wastewater, sewage, and feedlots (Carpenter et al., 1998; Schindler, 2006). While difficult to control, some practices have been enacted in several countries to restrict external nonpoint P sourced from agricultural runoff, contaminants (land use change development), unsewered urban runoff, and runoff from abandoned mines (Shortle and Horan, 2001). However, elimination of externally derived P does not always result in reduced P concentration and ecosystem recovery. Similarly, control of internal phosphorus loading must also be achieved (Cooke et al., 2016). Internal phosphorus loading is defined by Orihel et al. (2017) as all physical, chemical, and biological processes enabling bioavailable P mobilization from the benthic environment to overlying water.

Figure 1: *Eutrophication in the Netherlands. From Miquel Lürling, Wagenigen University and Research.*

Control of internal phosphorus loading requires locking P in biologically unavailable forms through chemical binding until it can be buried. Effective P burial requires stable binding under varying redox conditions, water hardness, and pH concentrations (Copetti et al., 2016). To this effect lanthanum and aluminum are redox stable phosphate (PO_4^{3-}) binders under most natural lake conditions while posing some eco-toxicological and human health risks (Copetti et al., 2016). The importance of iron (Fe) for phosphate fixation has recently become increasingly been recognized and has been proposed as an

additive for lake PO_4^{3-} fixation (Smolders et al., 2001; Guerts et al., 2008; Rothe et al., 2015; Orihel et al., 2017)). Due to its low toxicity risk, high natural abundance, and PO_4^{3-} binding iron has been viewed as a relatively natural and safe solution for PO_4^{3-} fixation. Despite this, irons redox instability poses challenges for efficient treatment. Fe coprecipitated PO_4^{3-} or PO_4^{3-} adsorbed to the iron (oxy-)hydroxide surface will be released upon ferric iron (Fe(III)) reduction. Long-term iron fixation is also achieved through ferrous iron (Fe(II)) fixation as vivianite. Accordingly, the conditions leading to long-term Fe(III) bound P fixation and vivianite formation are important for effective remediation projects, yet both are not fully understood (Stigebrandt et al., 2014; Rothe et al., 2015). Additionally, the presence of dissolved humic compounds have been found to reduce metal phosphate precipitations (Inskeep and Silvertooth, 1988a, 1988b) while results from Kleeberg et al., (2012) also indicate organic matter (OM) and sulphate (SO_4^{2-}) control on iron binding P processes. Long-term Fe-PO_4^{3-} binding mineral vivianite is present in many aquatic environments and stable in 6 to 9 pH ranges found in natural waters (Nriagu, 1972; Rothe et al., 2016). Conversely, competition for PO_4^{3-} or Fe by calcium (Ca), sulfide (S^{2-}) and magnesium (Mg) may further impede vivianite mineralization, while having mixed results for phosphate fixation (Kirk et al., 1990; Smolders and Roelofs, 1993; House and Denison, 2000). Few conclusions about the redox cycling and long-term formation of iron-phosphorus minerals in high OM flux lakes have been made which necessitates further investigation.

In view of irons benefit for P fixation, it has been added to several lakes across Europe (Rothe et al., 2016; B-Ware, 2018[1]; Quaak et al., 1993; Ter Heerdt et al., 2012; Waterschap Friesland, 1995[1]; Wolter, 2010; Kleeberg et al., 2012; Kleeberg et al., 2013; Deppe and Benndorf, 2002). However, mixed treatment results have prompted discussion and research on iron's redox instability under varying water hardness, pH, and redox conditions (Cooke et al., 1993; Jaeger, 1994; Gunnars et al., 2002; Gulati and van Donk, 2002; Gächter and Müller, 2003; Hansen et al., 2003; Smith et al., 2011; Kleeberg et al., 2012; Ter Heerdt et al., 2012; Kleeberg et al., 2013; Copetti et al., 2016). As a result, high OM and SO_4^{2-} fluxes, or other factors may be posing barriers to efficient P binding in shallow lakes. Despite several Dutch lake iron treatments, there has been no examination on the long-term effects of sediment P binding.

These findings suggest relationships between OM, surface water, porewater, and sedimentary concentration for long-term P fixation. Yet, the above traits in iron treated lakes has been seldomly investigated. It is therefore the purpose of this project to provide verifiable data, calculations, and interpretations of P binding activity in several lakes. Namely, iron cycling, burial reactions, and long-term iron storage are under examination.

1.1 Objectives

This project focuses on iron and phosphorus in shallow lake sediments. Investigation will target interactions of iron and phosphorus indicative of P trapping, specifically iron cycling and long-term iron storage. In addition, recovery of treatment iron will be investigated. In this way the project aims to answer the following questions:

1. **What quantity of treatment iron is visible in the sediments?**
2. **Has iron addition affected the redox zonation in treated lakes?**
3. **Has iron addition increased P trapping by the ferrous wheel and vivianite formation?**
4. **What are the likely Fe and P species in the treated lake sediments?**

[1] Authorship was not provided in this techincal report. The organization and publication year are therefore referenced.

2. Background

2.1 Biogeochemistry in early aquatic sediments

The Earth is regarded as a giant biogeochemical system (Schlesinger and Bernhardt, 2013) of which human activities have affected the water, carbon, nitrogen, phosphorus, and sulfur cycles (Stumm and Morgan, 1996). Water-logged sediments composed of organic and inorganic matter represent a stage within (bio)geochemical cycles that are susceptible to degradative processes. OM production is driven by photosynthesis which largely influences nutrient transport to the sediments. Due to early degradation a combination of biotic and abiotic processes changes the quantity and quality of sedimentary OM. As abiotic organic matter (OM) degradation is slow, microbial respiration is the principle form of 'early diagenesis' and OM remineralization (Stumm and Morgan, 1996; Raiswell and Canfield, 2012). Microbes gain metabolic energy for respiratory processes through energy-yielding redox reactions over which redox zonation is controlled by specific microbial reducing enzymes and the Gibbs

Table 1: *Processes, reactions, and standard state Gibbes free energy change for the exergonic reactions. From Burdige, 2011.*

Process	*Chemical reaction*	*ΔG° (kJ mol C^{-1})[b]*
Aerobic respiration	$C_6H_{12}O_6 + 6O_2 \rightarrow 6CO_2 + 6H_2O$	–471
Organotropic denitrification	$5C_6H_{12}O_6 + 24NO_3^- \rightarrow 12N_2 + 24HCO_3^- + 6CO_2 + 18H_2O$	–444
Organotrophic manganese reduction	$C_6H_{12}O_6 + 18CO_2 + 6H_2O + 12\delta\text{-}MnO_2 \rightarrow 12Mn^{2+} + 24HCO_3^-$	–397
Organotrophic iron reduction	$C_6H_{12}O_6 + 42CO_2 + 24Fe(OH)_3 \rightarrow 24Fe^{2+} + 48HCO_3^- + 18H_2O$	–131
Sulfate reduction	$2C_6H_{12}O_6 + 6SO_4^{2-} \rightarrow 6H_2S + 12HCO_3^-$	–76
Methanogenesis	$2C_6H_{12}O_6 \rightarrow 6CH_4 + 6CO_2$	–49

free energy yield for each mole of oxidized organic carbon by the respective terminal electron acceptors (Table 1) (Froelich et al., 1979; Stumm and Morgan, 1996). Sequential removal of nitrate (NO_3^-), manganese(II) (Mn(II)), Fe(II), and SO_4^{2-} results in sedimentary vertical redox stratification (Table 5). Microbial reduction produces ammonium (NH_4^+), Mn(II), Fe(II), H_2S, and CH_4 as shown in the biogeochemical redox model and redox reactions (Figure 2; Table 1).

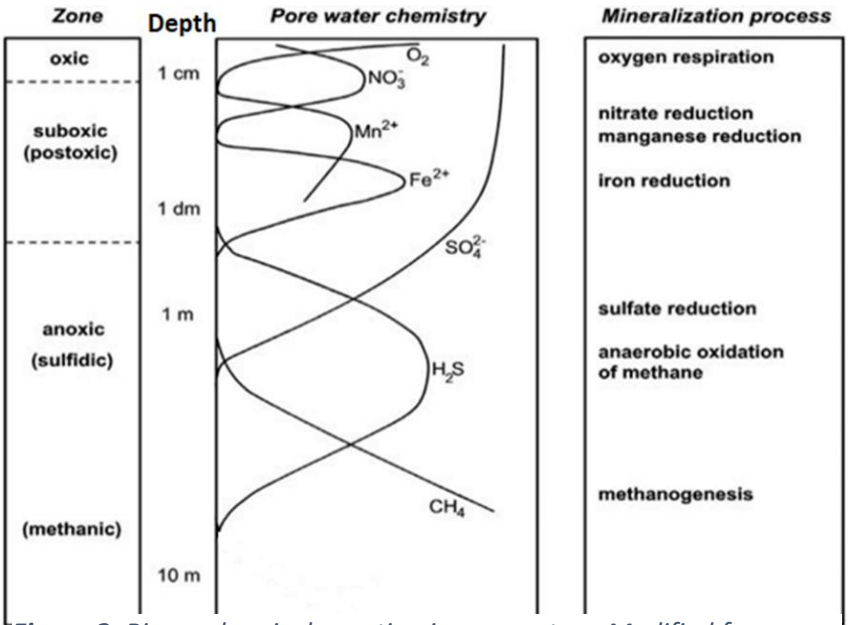

Figure 2: *Biogeochemical zonation in porewaters. Modified from Jorgensen and Kasten, 2006.*

Oxygen is the thermodynamically preferred electron acceptor and its water/sediment column availability primarily controls the reduction zonation of other molecules. However, depending on the stability of

terminal electron acceptors, simultaneous reductions are possible (Postma and Jakobsen, 1996). Sediment oxygen availability is limited by transport processes from bioturbation, bioirrigation, mixing, and anthropogenic irrigation (Jones and Welch, 1990; Cai and Sayles, 1996; Burdige, 2006). Additionally, seasonal algae blooms and high nutrient availability can exacerbate oxygen depletion (Hutchinson, 1957; Anderson and Garrison, 1997). Biogeochemical zonation drives mineralization in early sediments. Aqueous phases will precipitate according to oversaturation to respective minerals and reaction rates. Mineral stability depends on temperature, solubility, biotic interaction, and pH concentration (Strumm and Morgan, 1996).

2.2 Iron geochemistry

Natural iron is mainly found as a dissolved or solid form for the Fe(0), Fe(II), and Fe(III) redox states. The iron cycle is complex as fluxes cannot include simply dissolved and solid species. Aquatic iron size fractionation is not strict and is defined as colloids (<1 µm diameter), nanoparticles (<0.1 µm diameter), and aqueous species (<0.02 µm diameter) (Raiswell and Canfield, 2012). Practical definitions are based around filterable size fractions where >1.0 µm is particulate, <0.45 µm is colloidal, <0.2 µm is mainly nanoparticles, and <0.02 µm represent aqueous species (Figure 3) (Raiswell and Canfield, 2012).

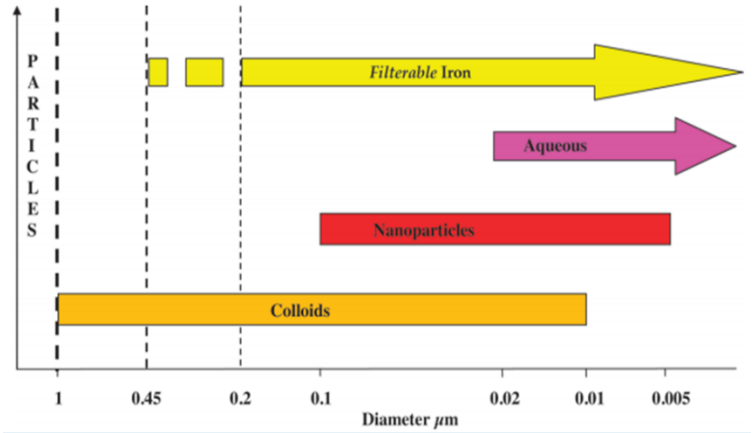

Figure 3: *Size ranges for aquatic iron. From Raiswell and Canfield, 2012.*

Fe(III) is commonly associated with silicates or as one of 16 iron (oxy-)hydroxides (Appendix 1), henceforth iron (oxy-)hydroxides will be collectively referred to as iron oxides. Iron oxides are found primarily as

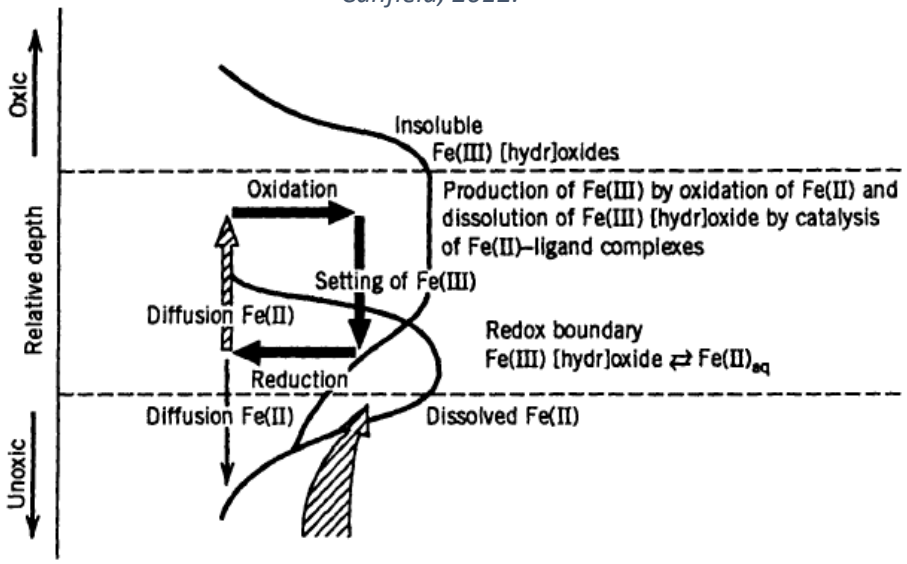

Figure 4: *Fe(II) and Fe(III) redox transformation at the oxic and anoxic boundary in water or sediments. From Stumm and Morgan, 1996.*

solids and are insoluble in water and require. However, complexation with organic ligands increases their solubility and bioavailability (Sholkovitz and Copland, 1981; Stumm and Morgan, 1996). Upon increasingly anoxic conditions Fe(III) will be reduced to Fe(II) (Figure 4).

2.2.1 Fe cycling

Reduced Fe(II) is stable in dissolved form in anoxic waters where it will diffuse upwards and downwards according to concentration gradients (Stumm and Morgan, 1996; Raiswell and Canfield, 2012). The mineral class, names, and chemical formulas for important biogeochemical cycling Fe minerals are given in table 2.

Table 2: *Important BGC iron minerals. From Raiswell and Canfield, 2012*

Mineral Class	Mineral Name	Formula
(Oxyhydr)oxides	Ferrihydrite	$Fe_4HO_8.4H_2O$
	Lepidocrocite	γ-FeOOH
	Goethite	α-FeOOH
	Haematite	Fe_2O_3
	Magnetite	Fe_3O_4
(Oxy)hydroxyl-sulphate	Schwertmannite	$Fe_3O_8(OH)_{1-1.8}.\ 8H_2O$
Sulphides	Pyrite	FeS_2
	Mackinawite	FeS
	Greigite	Fe_3S_4
Carbonates	Siderite	$FeCO_3$
Phosphates	Vivianite	$Fe_3(PO4)_2.\ 8H_2O$
Silicates : 7 Å Minerals	Kaolinite	$Al_2\ Si_2\ O_5\ (OH)_4$
Silicates: 10 Å Minerals	Illite	$(K, H_3O)\ (Al, Mg, Fe)_2\ (Si, Al)_4\ O_{10}\ (OH)_2\ (H_2O)$
Silicates: 14 Å Minerals	Smectite	$(Ca, Na)\ (Al, Mg, Fe)_2\ (Si, Al)_4\ O_{10}\ (OH)_2.\ x\ H_2O$
	Chlorite	$(Mg, Fe, Mg)_6\ (Si, Al)_4\ O_{10}\ (OH)_8$

Upward diffusion will lead to abiotic recycling of Fe(II) to Fe(III) as a function of oxygen availability, pH, and electron activity (Davison, 1985; Burley et al., 2001). Fe(II) oxidation occurs abiotically and biotically through aerobic and anaerobic processes (Figure 5) (Ghiorse, 1984; Ionescu et al., 2015; Straub et al., 1996; Straub et al., 2001). Due to seasonal decreases in pH and temperature, lower abiotic groundwater

Fe(II) oxidation rates are present in winter while increased pH and temperature in summer raise Fe(II) oxidation rates (van der Grift et al., 2014); this relationship is likely present in lake ecosystems.

Downwards diffusion will result in Fe(II) precipitation according to equilibrium concentrations and rate limiting precipitation processes. Bound Fe(II) is commonly associated with carbonates, sulfides, and phosphates. Fe(II) minerals are stable in anoxic environments.

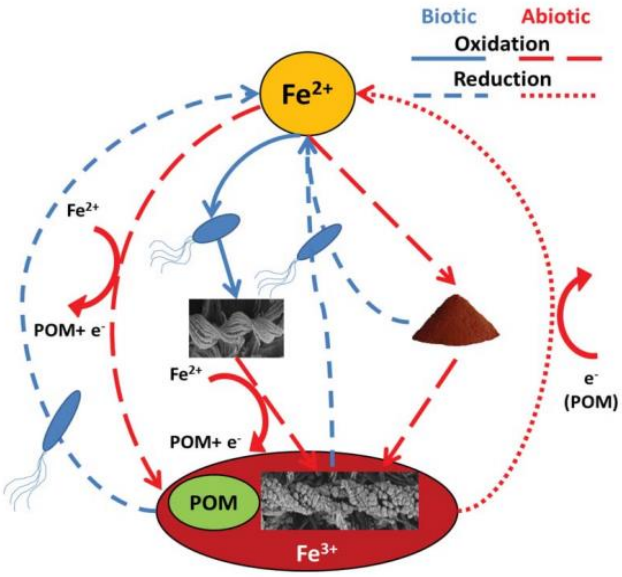

Figure 5: *Conceptual model of biotic and abiotic iron oxidation, reduction, sorption, and precipitation. The two stocks (photos within the figure) represent iron-binding organic matter. The iron mount represents iron oxidized abiotically without OM involvement. From Ionescu et al., 2015.*

2.2.2 P trapping

P occurs predominantly as $H_2PO_4^-$ and HPO_4^{2-} in lake environments with natural pH values between 5-9 (all PO_4 containing species will be collectively referred to as phosphate or PO_4^{3-}). Effective Fe bound P trapping occurs through the ferrous wheel and authigenic vivianite formation (Figure 6). Fe will bind P differently according to the environment as denoted in the ferrous wheel model (Figure 6). In oxic environments, iron oxides are effective P sorbents due to their high specific surface areas, low solubility in water, and thermodynamic stability (Cornell and Schwetmann, 2003; Strumm and Morgan, 1996). In the ferrous wheel, anoxic zone dissolved P will be released from the solid phase primarily due to iron(III) reduction and OM degradation where it will be transported upwards or downwards by advection or diffusion. Released dissolved P transported upward will bind to the surface of iron oxides whereas downwards P transport to anoxic layers will structurally bind to iron as authigenic vivianite ($Fe_3^{II}(PO_4)_2 \bullet 8H_2O$) (or other authigenic minerals). The reductive reaction for vivianite formation (Stumm and Morgan, 1996):

$$(Fe_3O_4)_{(s)} + 2H_2PO_4^- + 4H^+ + 2e^- = (Fe_3(PO_4)_2 * 8H_2O)_{(s)} \quad (1)$$

Authigenic vivianite formation will trail iron(II) sulfide (FeS_x) formation (Smolders and Roelofs, 1993; Kleeberg et al., 2012), representing its precipitation following sulfide removal according to the following reaction (Berner, 1970):

$$Fe_3(PO_4)_2 * 8H_2O + 3H_2S \leftrightharpoons 3FeS + 2H_2PO_4^- + 8H_2O + 2H^+ \quad (2)$$

In sulfidic sediments Fe(II) will bind to sulfide (S^{2-}) following sulphate (SO_4^{2-}) reduction, producing pyrite (FeS_2) as a terminal product (Stumm and Morgan, 1996). The overall reaction for pyrite formation (Berner, 1981):

$$3H_2S + S^0 + Fe_2O_3 = 2FeS_2 + 3H_2O \quad (3)$$

If Fe concentration is enough to bind P, further OM P release and transport would increase authigenic vivianite formation or P associated with the ferrous wheel. In methanic sediments rich in organic matter, siderite ($FeCO_3$) and vivianite may precipitate (Berner, 1981). The overall reaction for siderite formation (Curtis et al., 1986):

$$7CH_2O + 2Fe_2O_3 = 3CH_4 + 4FeCO_3 + H_2O \quad (4)$$

Fe removed through non-ferrous phosphate authigenic mineralization would require an import of reactive Fe from the sediments or external sources for sustainable ferrous wheel and vivianite P binding.

In the interrupted ferrous wheel, influx of degradable organic matter bound P and/or increasing sulfidic conditions limit efficient iron bound P trapping (Figure 6). As OM deposition is high, phosphate release due to OM degradation will exceed the removal of P from the sediment by authigenic mineral formation resulting in the saturation of the ferrous wheel. Increasing surface water sulphate concentration will result in deepening of the of the sulphate reduction zone due to rate limiting sulfate reduction. As a result downward transport of dissolved Fe(II) will be exhausted predominantly by authigenic FeS_x formation increasing solid phase iron and sulfur in the anoxic layer. Consequently, internal P loading will occur freely.

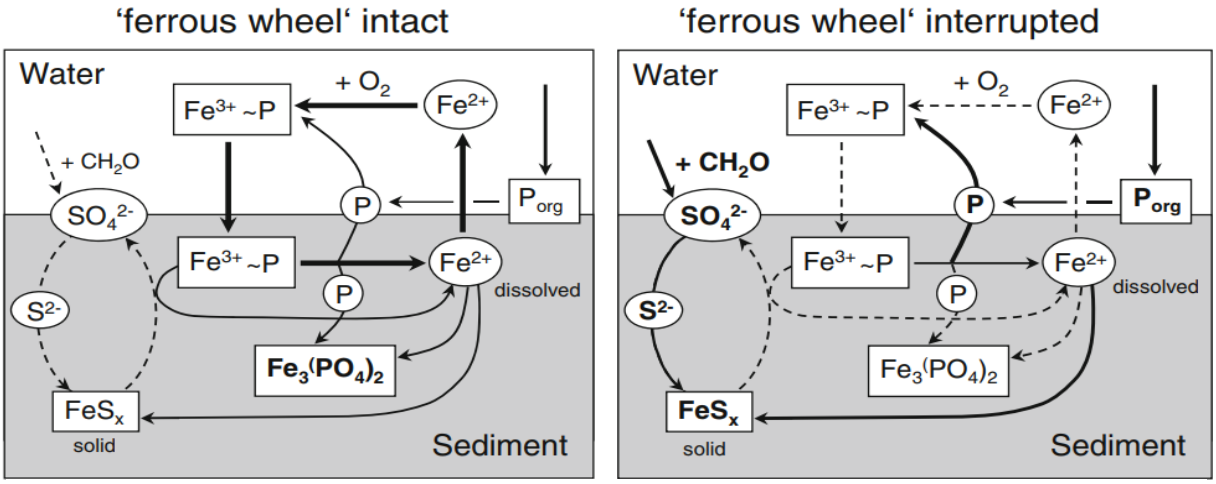

Figure 6: *Iron cycling and P binding model at the sediment water interface. Solid compounds are in rectangle boxes. Ovals/circles represent dissolved species. Dotted lines represent minor processes in the respective situations. Solid lines and their respective thickness represent the importance of the process within the situation. Organic matter (represented as CH_2O and sulphate are introduced on the left of each figure. Sulfate reduction increases the S^{2-} content in the sediments.* ***The left panel*** *represents a low sulphate and low organic matter system in which phosphate is adsorbed and on the surface of ferrous wheel cycling Fe^{3+} and fixed as both vivianite and FeSx.* ***The right panel*** *describes a high sulphate and high organic matter system in which iron preferentially forms FeSx minerals. Functioning of the ferrous wheel occurs through sediments associated with continuous Fe^{3+} and Fe^{2+} cycling. From Kleeberg et al., 2012.*

3. Materials and Methods

3.1 Study sites

Landscape background

The Netherlands is a very flat country that is below or close to sea level. During the Pleistocene much of present-day Netherlands was submerged. Holocene fluvial sediment deposits slowly built up the land from which sandy coasts, mudflats, salt marshes and peat bogs developed (Hoeksema, 2007). By AD 800 - 1000 much of the country was covered by marshy clays, peats, and lakes for which peat has been an important fuel source in historical communities.

A significant land portion has been reclaimed from the sea and salt marshes for agricultural use for which present day water cover stands at about 16% (Ter Heerdt et al., 2012). Water covers a total area of 41, 864 km^2, 12,650 km^2 of which is shallow (<2m) peat lakes (Ter Heerdt et al., 2012) originating from dredging and peat removal. Dutch lakes are primarily located in the North, North-West, and western parts of the country as part of the catchment areas of the Rhine, the Meuse, and the Scheldt Rivers. Although much peat has been removed, many shallow lake environments still contain a large amount of peaty material. During summer months they are a reservoir for agriculture and canal water balance while winter precipitation replenishes the system. As a natural ecosystem, shallow peat lakes are hosts to many migratory birds and wetland species for which sediment disturbance from wind-wave action, outboard engines, and bioturbation is estimated to be about 15 cm (Quaak et al., 1993). Sampling locations within the Netherlands are shown in figure 7. Iron treatment information is provided in table 3[2].

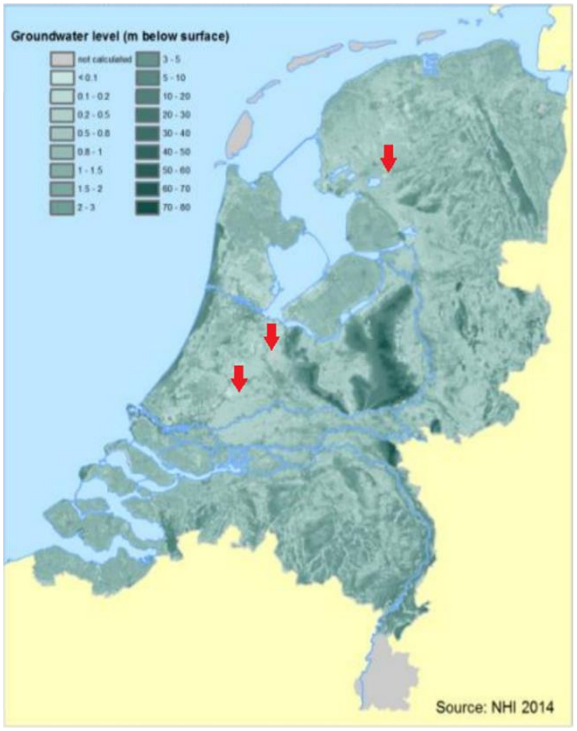

Figure 7: *Map of the Netherlands with the respective approximate sampling locations. Land cover color indicates groundwater water below the surface. Note legend in the top left. From NHI 2014.*

3.1.1 Reeuwijk Lakes

The Reeuwijk lakes are the result of 17th century peat extraction forming a lake complex. Located nearby to the city of Gouda, these lakes are urbanized and host surrounding residences and businesses. The soils of this region are categorized as peat soils and generally feature a high amount of organic matter. Sediments of these lakes are classified as loosely bound and prone to bioturbation. The lakes are interconnected except for Sloene and Klein Vogelenzang. The lakes are open to electric motorboats

[2] Specific $FeCl_3$ solution treatment information was not regularly provided in available reports. A 40% solution was used in Nannewijd and other lakes likely used a similar solution concentration.

which are a cause of sedimentary disturbance. Sampling locations within the Reeuwijk lakes are shown in figure 8[2].

Gravenbroek (Dutch: 's-Gravenbroek)

Located in the western zone of the Reeuwijk lakes, Gravenbroek (GK) covers 105.22 hectares and is surrounded by other lakes from the North, South, and East (Brouwer Group, 1993[1]). Gravenbroek has not been treated with iron nor dredged. Sediments are reportedly loose and sulfide rich (B-Ware, 2018[1]). Maximum depth is 2.8 m and average depth is 2.1 m (Brouwer Group, 1993[1]). Unlike the other lakes in this system, Gravenbroek does not serve a primary purpose as an ecological zone, but rather as a recreation and residential area (Torenbeek, 2013).

Sloene

Located in the north-west quadrant of the Reeuwijk lakes, Sloene (SL) covers an area of about 9.21 hectares and is surrounded from the North, East, and South by other lakes all of which feature a loose and sulfide rich sediment type (B-Ware, 2018[1]). Previously Sloene lake was connected to the lake complex water flow but has been disconnected before iron treatment. Additionally, ground water from lake Broekvelden has been exported to Sloene; Broekvelden waters may contain byproducts of past drug manufacturing (personal communication Bart Schaub, Hoogheemraadschap Rijnland).

Background iron concentration in the top 5 cm of sediment is averaged at 22 g Fe kg^{-1} (B-Ware, 2018[1]). Lake water pH is relatively high varying between 9.8 to 7.2 since 2005 with a temporal average at 8.14 (B-Ware, 2018[1]). Due to high concentrations of surface water phosphorus, management treated the lake with iron chloride ($FeCl_3$) in 2014 until 2017. Iron chloride was gradually introduced to the lake habitat in a system that was modelled after the Terra Nova treatment (see: Loosdrecht lakes) (personal communication Bart Schaub, Hoogheemraadschap Rijnland). Total treatment iron was

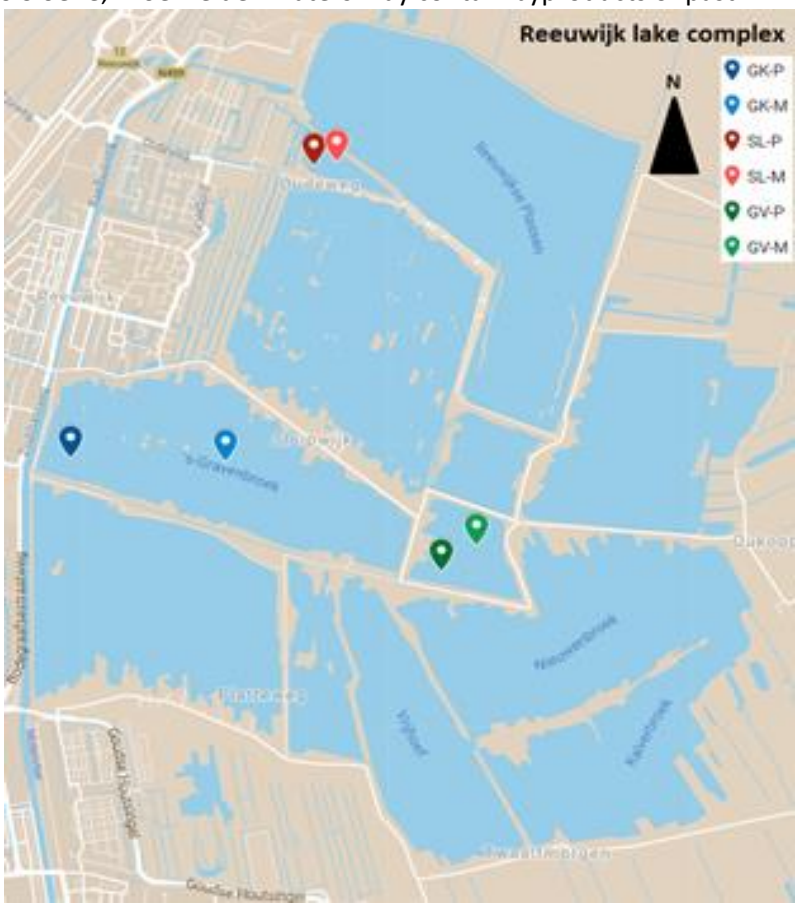

Figure 8: *Reeuwijk lake complex and sampling locations for Gravenbroek (GK), Sloene (SL), and Groot Vogelenzang (GV). Note the legend in the top right. Blue markers indicate untreated reference lake.*

178.3 g Fe/m^2 (Frank, Tableau Public, 2019[3]).

Following treatment, iron in sediments was found to be strongly correlated to both phosphorus and sulfur (B-Ware Sloene, 2018[1]). During iron treatment sulfate concentrations in the porewater have increased during spring and decreased in summer, which is attributed to OM degradation (top 0 to 5-10 cm below the sediment water interface (SWI), averaged over 7 sampling locations) (B-Ware Sloene, 2018[1]). Since treatment, overall sediment phosphorus concentration is about 1.1 g P/kg and there is an apparent decrease in water productivity (B-Ware, 2018[1]).

Groot Vogelenzang

Groot Vogelenzang (GV) is in the eastern central part of the Reeuwijk lake system. Surface area covers an area of about 18 hectares with a max depth of 2.5 m and a 1.75 m average depth. The sediments are very loose, and the water retention time is 35 days (Quaak et al., 1993). Reported average sediment composition analysis in the top 5 cm found a 93.8% w/w moisture content, 49% organic matter content (loss on ignition, a pH of 7.4, total P of 1.6 mg / g, total Fe before treatment of 24 mg / g (Quaak et al., 1993). An iron(III) chloride solution was applied directly to the lake bottom by water jets which mixed the top 15 to 20 cm of sediments. Full coverage of the lake was guaranteed by using a high precision positioning system. In 1989 sediments were treated at a rate of 2 to 3 ha per day with total treatment time of 3 weeks (Quaak et al., 1993). In total, 120 tons of 40% $FeCl_3$ were used amounting to 100 g Fe / m^2. After treatment the top 5 cm of sediments had on average 40 mg / g of total iron.

3.1.2 Loosdrecht Lakes

Located to the west of Hilversum the Loosdrechtse Plassen is a lake complex / wetland habitat reserve open to the public. These lakes are affected by cyanobacteria (blue-green algae) blooms likely due to

[3] This is the public access database for Sloene lake provided by Hoogheemraadschap Rijnland. “Frank” is the only author of the public access database.

eutrophic conditions stemming from high phosphate concentrations. The surrounding soils had naturally high iron concentrations which had controlled past phosphate loading. From December 2018, Loosdrecht inlet waters are treated with $FeCl_3$ (personal communication Gerard Ter Heerdt, Waternet). Sampling locations within the Loosdrecht lake complex are shown in figure 9.

Figure 9: *Loosdrecht lake complex and sampling locations for Terra Nova (TN) and Vuntus (VT). Note the legend in the top right. Blue markers indicate untreated reference lake.*

Terra Nova

The 85-hectare lake Terra Nova (TN) has been subject to several studies and recovery experiments. Notably this lake had experienced year-round algae blooms from 1987 to 2004 (Ter Heerdt et al., 2012). In 2003 to 2004, sediment disturbing bream were removed from the lake leading to a disappearance in cyanobacteria and clearing of winter and spring algae blooms. Increased phosphate concentrations in 2005 lead to the summertime appearance of other cyanobacteria species (Ter Heerdt et al., 2012).

In 2010 and 2011 a mobile dosing system of a 40% dissolved iron chloride solution was added by a sprinkler system to the lake surface water at a fixed location. Iron was continuously applied in low doses for a 1.5-year period. Distribution was achieved a windmill attached to a water pump where treatment iron was indirectly distributed by wind-controlled water currents. After treatment the lake was expected to be completely distributed with 33 g / m^2 of iron with the goal of observing reduced eutrophic conditions and benthic macrophyte development. Various sediment traps recorded an average of 28 g Fe / m^2 added between May 2010 and August 2011 (Ter Heerdt et al., 2012). Based on internal and external P fluxes iron addition was estimated to control eutrophic conditions for 26 - 42 years (Ter Heerdt et al., 2012).

As a result of the iron addition, the WFD score based on chl-a saw a 0.22 point increase which is expected to push the lake from a “poor” status to a “good” status. In 2014 TP and orthophosphate concentrations had returned to pretreatment levels (Chrzanowski et al., 2015). Despite this, chl-a concentrations remained low, algae blooms did not return, and macrophytes were developing properly

(Chrzanowski et al., 2015). During the summer of 2018 Algae blooms returned to the lake, ending treatment effectiveness (personal communication, Gerard Ter Heerdt, Waternet).

Vuntus

The 33-hectare lake Vuntus (VT) is in the eastern region of Loosdrecht. Vuntus serves as a recreational area and is open to motor boats. Average depth is reported at 1.4 m and prevailing winds originate from the South-West. Due to wind patterns, the South-West of the lake receives high amounts of sediment deposition. The lake features mostly loose sediments in the South-West while hard sand layers can be found in the center of the lake. Background iron concentration is 22 g Fe/ kg sediment (Boers, 1991).

3.1.3 Friesland lakes

Nannewijd

The 115-hectare Nannewijd (NW) nature reserve is a recreational zone and water bird stopover point. The 100-hectare lake is the result of peat digging and has an average depth of about 80 cm. Prominent winds approach Nannewijd from the South-West directing the loose and sandy sediments to accumulate in the South, South-West, and northern canal district of the lake. On Nannewijd's eastern side more tightly packed sediments can be found. Historically, the regions soils are known to have been iron rich and are thought to have had a delaying effect on eutrophic conditions. Sustained eutrophic conditions indicate that soil iron leachates had been depleted. Beginning in 1993 Nannewijd underwent several restorative treatments:

1. **Hydrological isolation:** Reduction in the inflow and outflow of the lake, effectively increasing the water retention time.
2. **Dredging:** 100,000 m^3 of sediment and sludge was removed from the lakebed where sludge was thicker than 10 cm (about 25 % of lake area).
3. **Phosphate fixation with $FeCl_3$:** Every square meter was treated with ferric chloride. Amount of ferric chloride used depends on the sludge layer thickness: 0-5 cm, 10.7 g Fe/m^2; 5-10 cm, 32.1 g Fe/m^2; >10 cm, 53.5 g Fe/m^2.
4. **pH correction with calcium hydroxide:** The phosphate fixation treatment significantly reduced the pH of lake waters (due to low buffering capacity) therefore $Ca(OH)_2$ was used to prevent acidification.
5. **Biomanipulation:** Removal of zooplanktivorus and sediment disturbing bream/carp for 3 months during mid-summer.
6. **Inlet water filter and fixation:** Inlet waters were passed through an 18-hectare reed (helophyte) filter with 3 plants/m^2 followed by a 15 mg Fe/L treatment to remove residual phosphorus (total amounts are not given) (Veeningen, 1996).

Ferric-chloride addition started in October 1994 following completion of dredging measures. Accurate application was controlled through a high-resolution tracking system ensuring complete lake coverage. Overall, the iron concentration in the sediments increased by 80% (Waterschap Friesland, 1995). These measures resulted in significant 1993 to 1996 changes in transparency, total phosphate, chlorophyll-a, and total nitrogen. As of June 2018, the two-year average has shown continued water quality improvements. Sampling locations within Nannewijd are shown in figure 10.

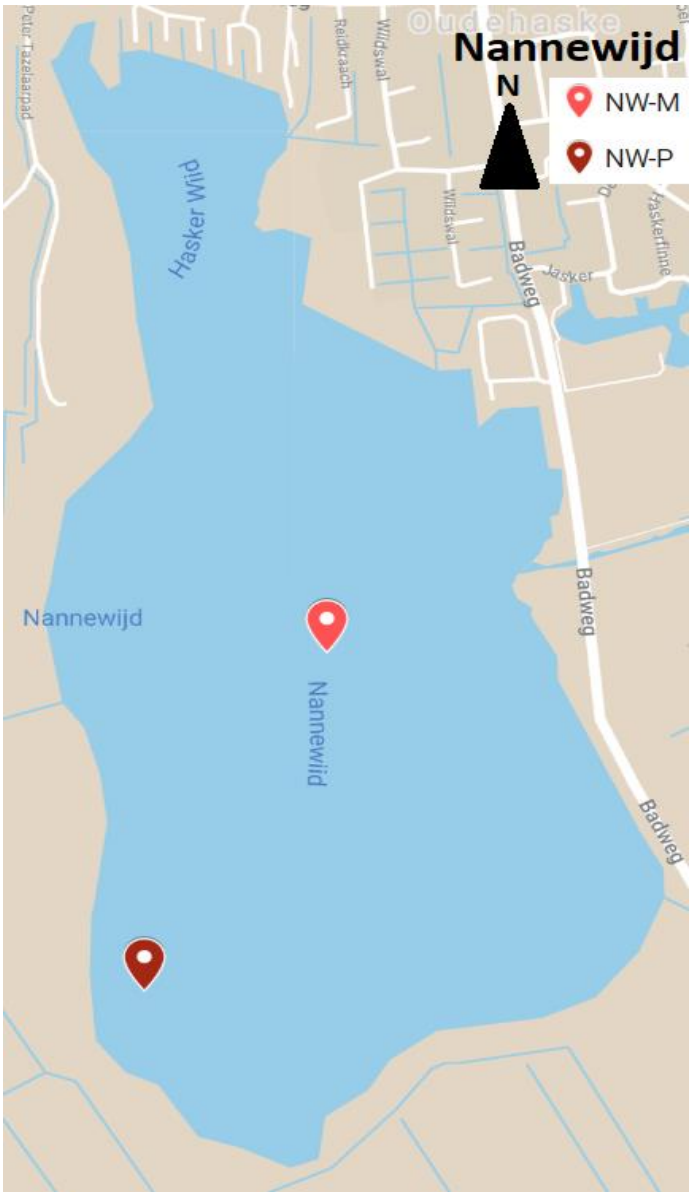

Figure 10: *Friesland lakes, lake Nannewijd (NW). Note the legend in the top right.*

Botmeer

The 33-hectare lake Botmeer (BM) sits on a 55-hectare lake area. The lake shares the same catchment area with Nannewijd and has not been treated for phosphate fixation. The lake features a maximum depth of 4 m and an average depth of 50 cm. Water residence time is known to vary seasonally but is yearly averaged at 37 days. Lake Botmeer is closed to the public and is surrounded by pastures and farmland.

In 1994 lake Botmeer was found to have non-serious sediment pollution from zinc contamination, the pollution did not require restorative measures (the source is not known to this author). Sediments are of the peat type and analysis revealed two distinct layers: a top sludge layer and a bottom sludge layer. These sediments contained 14.6 % and 9.39 % (w/w) dry matter respectively and had loss on ignition (organic matter) values of 39 % and 66 % respectively in the middle of the lake (Witteveen & Bos, 2012). Bottom sediment contains about double the sulfur concentration compared with iron and observes a Fe / S ratio of less than 0.5 (Witteveen & Bos, 2012[1]). Thus, due to the slightly reducing conditions of peat soils/sediments (Witteveen & Bos, 2012[1]) under anaerobic conditions iron is expected to be bound to sulfur and have very little influence in phosphorus locking. Sampling locations within Botmeer are shown in figure 11.

3.2 Field materials and methods

Sediment core samples were taken over three sampling days from four lakes treated with iron and three which have not had iron treatment (Table 3). Shore-ward and lake middle sampling sites were chosen for their difference in sediment condition and prevailing wind-controlled sediment deposition. Samples were taken from Reeuwijk, Loosdrecht, and Friesland on November 14th, 2018, November 27th, 2018, and December 11th, 2018 respectively. Surface water electrical conductivity, dissolved oxygen, and pH were determined using a WTW Cond 3110, WTW ProfLine Oxi 3310, and WTW pH 3310 meters respectively, all devices had been calibrated the afternoon before fieldwork. Surface water samples were 0.2 µm syringe filtered with new filters into new 50 ml Greiner polypropylene centrifuge tubes. Surface water samples were subsampled for alkalinity, sulfide, and ion chromatography determination before the remainder was immediately 1% (volume/volume) acidified using 3.75 M nitric acid (HNO_3). Secchi disk depth was used to measure turbidity.

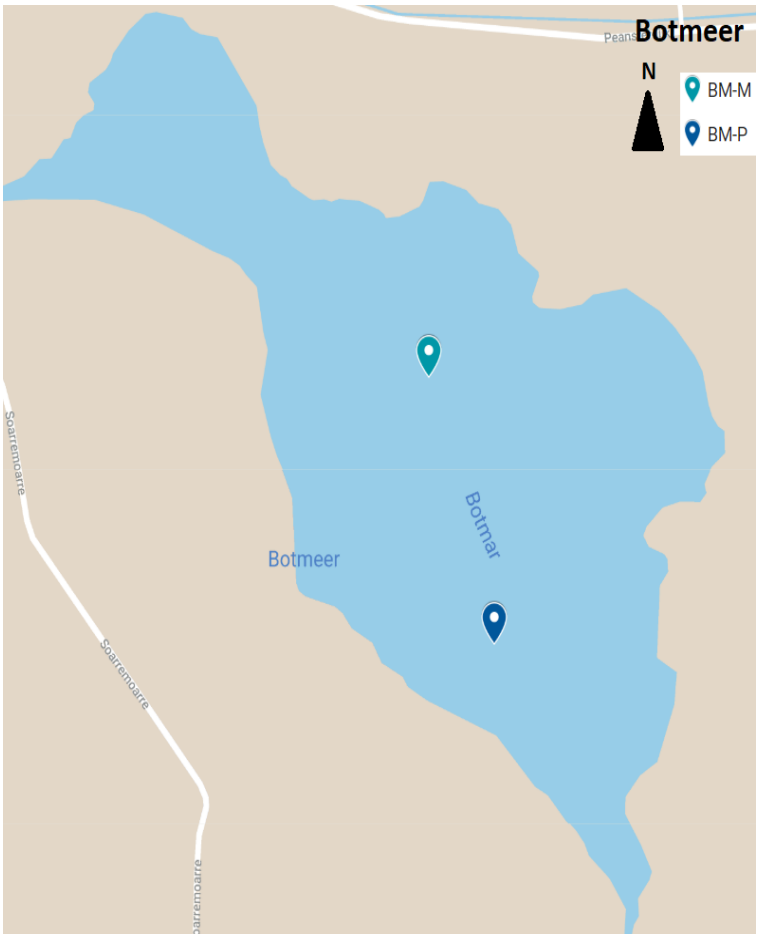

Figure 11: *Friesland lakes, Lake Botmeer (BM). Note the legend in the top right.*

To preserve surface water quality, sediment core sampling followed surface water measurements. Core samples were taken with a UWITEC piston gravity corer using predrilled transparent 60 cm long Plexiglas tubes roughly 6 cm in interior diameter (Figure 12). Pre-drilled holes of 3 mm diameter were placed from the 5th to the 50th cm of the core and covered with a water-resistant PVC style yellow tape. A minimum of approximately 5 cm of water was left at the top of each core to preserve oxic/anoxic conditions in the core before being capped. Sometimes the top of the sediment layer was not immediately clear, thus porewater sampling was chosen to contain the mostly permanent sludge layer. Porewater sampling depths averaged around the midpoint of a layer for the appropriate intervals (e.g. a data point at 10 cm

Table 3: *General parameters and treatment method for all lakes. Note the treatment location. Note Nannewijd treatment quantity.*
0 no treatment
+ to +++++ indicates strong similarity between recovered Fe between (P) and (M) cores in a lake on an increasing scale.
**** indicates strong similarity between BM cores.*

Region	**Reeuwijk**						**Loosdrecht**				**Friesland**			
Lake	**Gravenbroek**		**Sloene**		**Groot Vogelenzang**		**Vuntus**		**Terra Nova**		**Botmeer**		**Nannewijd**	
Core position in lake	Shore-ward	Middle	Shore-ward	Middle	Shore-ward	Middle	Shore-ward	Middle	Shore-ward	Middle	Shore-ward	Middle	Shore-ward	Middle
Core identifier	**GK-P**	**GK-M**	**SL-P**	**SL-M**	**GV-P**	**GV-M**	**VT-P**	**VT-M**	**TN-P**	**TN-M**	**BM-P**	**BM-M**	**NW-P**	**NW-M**
Sampling coordinates	52.0382141, 4.7230837	52.0380607, 4.7343453	52.0522319, 4.7407230	52.0523697, 4.7422917	52.0328666, 4.7498438	52.0340743, 4.7524523	52.2087451, 5.0707376	52.2121471, 5.0745517	52.2188980, 5.0442334	52.2222686, 5.0402821	53.0725875, 5.8737454	53.0750803, 5.8725495	52.9425324, 5.8634189	52.9475280, 5.8673798
Surface area (ha)	105.22		9.21		18		88		85		33		86.99 (treated area)	
Average depth (m)	2.1		2.3		1.75		1.4		1.4		0.5		0.8	
Treatment	-	-	$FeCl_3$		$FeCl_3$		-	-	$FeCl_3$		-	-	$FeCl_3$	
Treatment quantity (g m^{-2})	-	-	**178**		**100**		-	-	**33**		-	-	**53.5 (on 12.01 ha)**	**10.7 (on 56.61 ha)**
Treatment Location	-	-	Surface waters		Top 0 to 15 - 20 cm of sediments		-	-	Surface waters		-	-	Water colum	
Treatment method	-	-	Wind driven microcurrent		Boat application to sediment		-	-	Wind driven microcurrent		-	-	Boat application to	
Treatment quantity verification	-	-	No		High accuracy location based positioning		-	-	No, wind driven microcurrent dispersal		?	?	High accuracy location based positioning	
Heterogenity of Fe treatment between cores	0		+		+ +		0		+ +		* * *		+ + + +	+
Average total lake treatment Fe recovery (%)	**-**	**-**	**87**		**244**		**-**	**-**	**99**	**99**	**?**	**?**	**530**	**530**
Start of treatment	-	-	Apr-2014		1989		-	-	2010		-	-	Oct-1994	
Treatment duration	**-**	**-**	**~ 3 years**		**~4 weeks**		**-**	**-**	**~1.5 years**		**-**	**-**	**5 months**	
Literature Background Fe (mmol/kg)	-	-	716 (top 0 to 5-10 cm)	603 (top 0 to 5-10 cm)	430 (top 0-5 cm)		-	-	394 (top 0-2 cm)		-	-	-	-
Water residence time	-	-	> 2 years		35 days		1.5 years		1 year		37 days		>2 years	
Literature reference	Brouwer Group, 1993; Torenbeek, 2013		B-Ware, 2018; Frank, Tableau Public, 2019[1]		Quaak et al., 1993		Boers, 1991; Van Liere et al., 1987		Ter Heerdt et al., 2012; Mettrop, 2009		Witteveen & Bos, 2012		Veeningen, 1996; Waterschap Friesland, 1995	

indicates a drill hole at 10 cm and porewater from 9.5 cm to 10.5 cm below the SWI). Rhizons were secured tightly to vertically held cores using a rubber gasket following piercing of the yellow tape from the top of the sediment layer. Porewaters were extracted via vacuum within a few hours of core sampling using 5 cm porous length using 0.15 µm pore size rhizon samplers (Rhizosphere research products). Extractions for Friesland were conducted in a top down method to avoid surface water intrusion of porewater samples, while some Reeuwijk and Loosdrecht samples were extracted out of order[4]. Porewater sampling started within the following time frames:

- Sloene cores between 30 minutes to 1 hour
- Groot Vogelenzang cores < 2 hours
- Gravenbroek cores < 2 hours
- Terra Nova cores <2 hours
- Vuntus cores < 1 hour
- Botmeer cores between 30 minutes to 1 hour
- Nannewijd cores < 1 hour

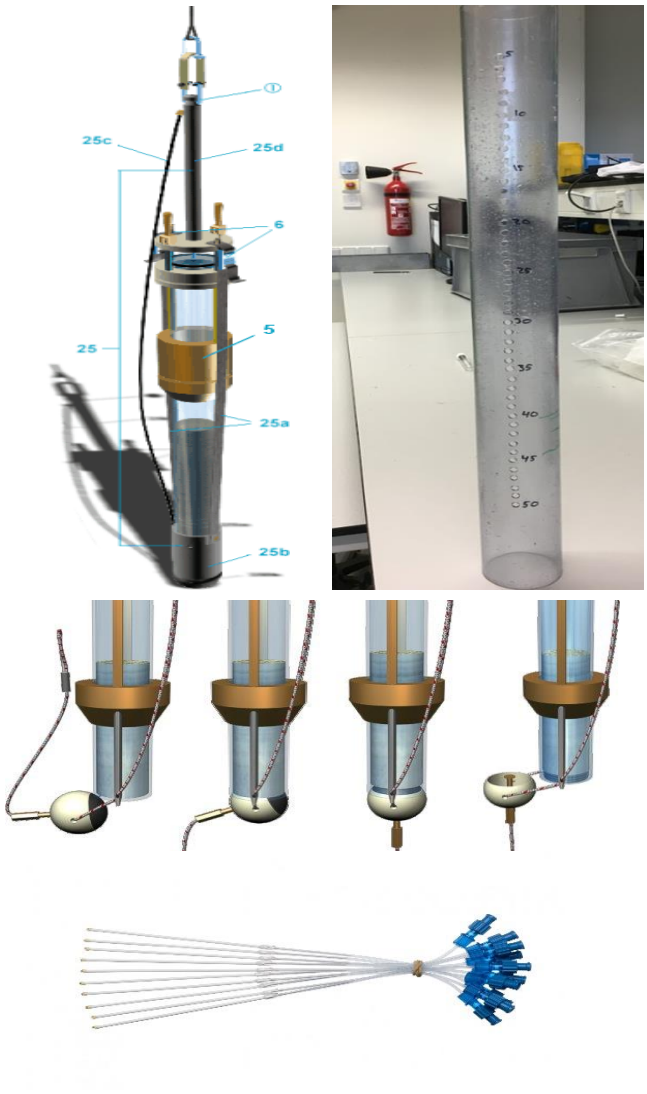

Figure 12: *Selected fieldwork materials. UWITEC piston gravity corer and locking mechanism (Top left and middle). Drilled Pexiglas cores (top right). Rhizons with 0.15 µm pore size (second photo from bottom). Photos from UWITEC; myself; UWITEC; Rhizosphere research products.*

[4] Some porewaters were extracted out of order due to errors made during early fieldwork. The most common error was connecting the vacuum syringe to the rhizon plug and not the porewater filtering section. This is due to the visual similarity between the rhizon/syringe connection point and the rhizon plug and the fact that both have the same diameter

Combinations of new and cleaned rhizons were used for porewater sampling. Rhizon cleaning did not have any observable effects on porewater composition. Rhizons were cleaned by sonication in 0.5 M nitric acid bath and pumped at a flow rate of 0.6 ml/min (Figure 14; Appendix 3). Porewater was extracted using the following procedure:

- Reeuwijk cores used exclusively new rhizons. Rhizon blocks extract up to 10 mL.
- Loosdrecht cores were sampled with a repeating pattern of two cleaned rhizons followed by one new rhizon, starting at the SWI. Rhizon blocks extract up to 5 mL.
- Friesland cores were sampled with a repeating pattern of two cleaned rhizons followed by one new rhizon, starting at the SWI. Rhizon blocks extract up to 7 mL.

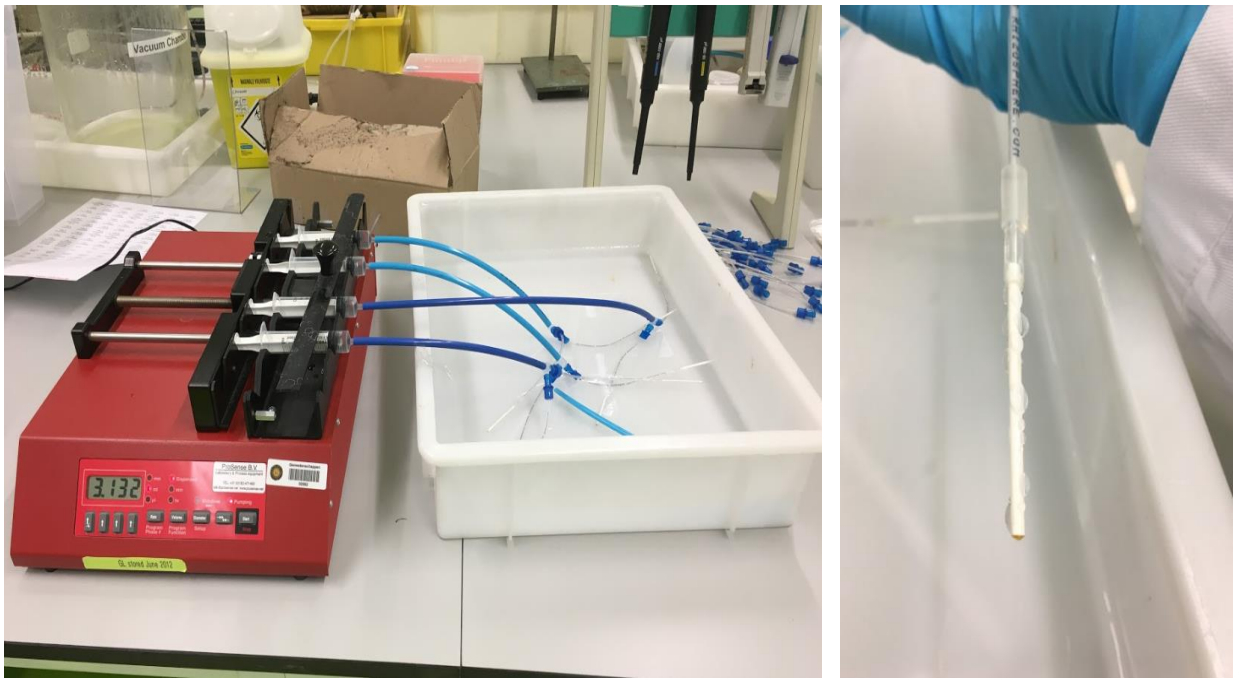

Figure 13: Left photo *Rhizon cleaning setup from a test run in which the flow rate was reduced and a total of 8 rhizons were attached. Cleaning was done on 4 rhizons at a time conncected to the 0.6 ml/min rate controlled pump.* ***Right photo*** *visual inspection of undamaged flow through rhizon filter.*

Porewater pH was determined directly after sampling by placing an aliquot on a DI water on a rinsed and paper towel dried petri dish and measuring the concentration using a Thermo Scientific Orion 9135APWP AquaPro Flat Surface pH electrode attached to an Eijkelkamp pH 18.37 meter.
Sulfide was measured on a Hach Field DR 2700 Spectrophotometer using the Hach Sulfide LCK 653 cuvette test. On each field day the sulfide spectrophotometer returned negative results. Subsamples were stored for alkalinity, sulfide, and ion chromatography before the remainder was stored in new 15 ml polypropylene Greiner centrifuge tubes and 1% acidified using 3.75 M nitric acid. Sediment cores were transported to the laboratory by car or van in a secured upright position. Surface waters, porewaters, and sediment cores were stored in refrigerators at 5 °C before analysis and core breakdown.

3.3 Laboratory methods

3.3.1 Surface and porewater analysis

All water samples were sent the next day for analysis by ion chromatography (IC) on a Metrohm 930 Compact IC flex with a Supp 7 with an anion guard and inductively coupled plasma atomic emission spectroscopy (ICP-OES) analysis within 24 hours of returning to the lab on a Spectro Arcos ICP-OES machine, samples were not immediately processed. Porewater alkalinity was determined spectrophotometrically using bromophenol blue[5] using an internal laboratory protocol, while surface water alkalinity was determined using the Gran-titration method (Sarazin et Michard et Prevot, 1999; Stumm and Morgan, 1996). Fe(III), and Fe(II) were determined spectrophotometrically using the ferrozine method (Viollier et al., 2000) following an internal lab protocol. Ammonium and phosphate (as orthophosphate) were quantified spectrophotometrically using internal laboratory protocols following the phenol- hypochlorite method (Koroleff, 1976) and the ascorbic acid method (Figure 14) (Koroleff, 1983). Due to variable porewater sample concentration, several dilutions were made for iron and phosphate spectrophotometric measurements after adequate range testing. Reagents for photometric measurements were mixed the day of analysis. Surface and porewater samples were gently mixed by rotating up and down before subsampling.

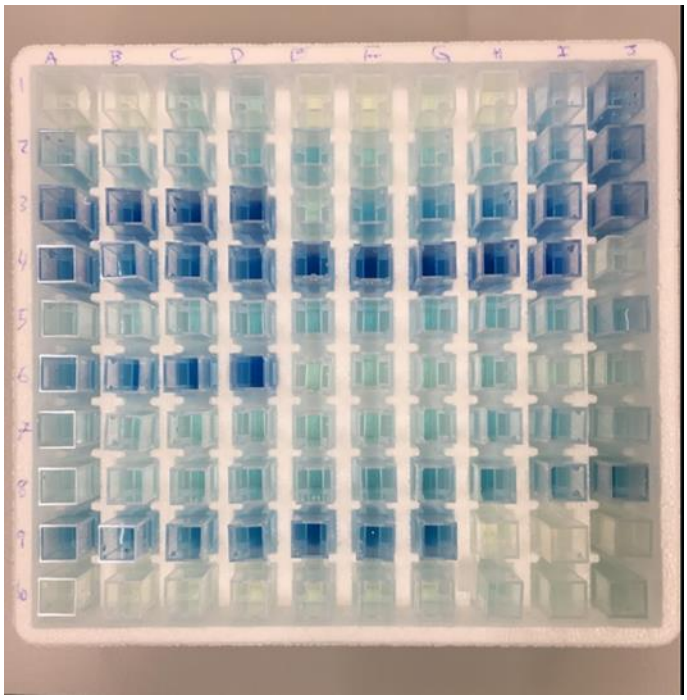

Figure 14: *Porewater filled microcuvettes for spectrophotometric measurement. Darker blue coloration indicates increasing reaction of acidified molybdate reagent with phosphate which is directly correlated to higher phosphate concentration.*

3.3.2 Core slicing

Sediment consolidation in sampled cores had taken place between sampling and laboratory-based core slicing. Sediment data corrections were made according to table 4. Sediment cores were processed in a glove-bag filled with N_2 gas (purged 4 times) and sliced into 1 cm sections and placed into new pre-weighed 50 ml Greiner polypropylene centrifuge tubes (e.g. a data point at 10 cm indicates sediment from 9.0 to 10.0 cm below the SWI and 14 cm indicates 13.0 to 14.0 cm below the SWI). Greiner tubes

[5] Reagents and calibrations were made using a 0.5 M Sodium Chloride solution. The method background indicates that salinity does not affect the measurement. Some agents in seawater are known to interfere with the measurement by catching some of the bromophenol blue color, it is not discussed if this is also the case in fresh waters.

were uncapped before being put in the glove-bag. Sediment layers were sliced in the following time frame[6]:

- Reeuwijk cores were processed 6 days after sampling.
- Loosdrecht cores were processed 9 days after sampling.
- Friesland cores were processed 7 days after sampling.

Table 4: *Layers of the sediment core that were expected to contain sludge matter were used to fill gaps caused by sediment core consolidation according to the following table. "SW" refers to the shore-ward core position and "Middle" refers to the middle of lake core. Core consolidation was absent in the Sloene Middle core.*

Sediment consolidation														
Lake	Sloene		Groot Vogelenzang		Gravenbroek		Terra Nova		Vuntus		Nannewijd		Botmar	
Core position	SW	Middle	SW	Middle	SW	Middle	SW	Middle	SW	Middle	SW	Middle	SW	Middle
Original layer (depth below SWI in cm)	Data point filled with data from the original core layer indicated below (cm)													
1	4	-	3	5	3	2	3	3	3	3	7	4	2	3
2	4	-	3	5	3		3	3	3	3	7	4	2	3
3	4	-	4	5	4		4	4	4	3	7	4		4
4	5	-	4	6	4		4	4	4		7	5		4
5	5	-		6							8	5		
6				6							8			
7											8			
8											9			
9											9			
10														

Following core slicing, sediment samples were weighed and frozen at -28°C. Filled Greiner tubes were dried using an anoxic freeze drier for 48 to 144 hours before being weighed again. Total sample freeze-drying time was determined by continued moisture presence after each 48-hour run. During freeze drying, many Greiner tubes cracked. Thus, several samples were transferred to a new Greiner tube in an argon atmosphere glovebox.

3.3.3 Sediment analyses

Sediment total carbon and total nitrogen were analyzed by CN elemental analyzer using a Carlo Erba NA1500 NCS using Dumas combustion and normal oven fillings. Samples were manually mixed by shaking before being subsampled using a clean and dry spatula into tin capsules. After weighing tin capsules were folded and drop tested on a clean surface for spills, samples with spills were remade.

Sample preparation for loss on ignition (LOI), X-ray fluorescence (XRF), and carbon/sulfur analysis (CS) was done using a Herzog HP-MA grinding using a Wolfram-Carbide vessel. LOI was determined by thermal gravimetric analysis (TGA) using a Leco TGA701 machine. XRF was analyzed using the pearl (XRF-P) fusion bead method on an ARL Perform'X machine. Fusion beads were prepared using 0.6 g of sample (after LOI, inclusive of SiO_2 for insufficient sample weight (see: 4.1 Data reliability)) and 6 g of flux (ICPH

[6] Core processing time frame depended on availability of core processing colleague, reparation status of core processing tools, and N_2 gas delivery.

Fluomix 6515 LiI). Fusion takes place at 1200°C. CS was prepared using 0.2 g of dried sample (see: 4.1 Data reliability).

3.4 Calculations

3.4.1 Surface and porewaters

Proton abundance (H^+ ion or hydronium ion), bicarbonate (HCO_3^-) , carbonic acid (H_2CO_3), and total aqueous inorganic carbon (TIC) were determined on surface and porewater samples (see: 3.2.0 - 3.3.1 Porewater analysis for surface and pore/water pH and alkalinity methods). Determination of H^+ was calculated from pH:

$$[H^+] = 10^{-pH} \tag{5}$$

In freshwater systems bicarbonate is the dominant source of alkalinity (Stumm and Morgan, 1996) and is here calculated as:

$$[HCO_3^-] = [alkalinity] \tag{6}$$

Carbonic acid is calculated as:

$$[H_2CO_3] = \frac{[H^+] * [HCO_3^+]}{K_1} \tag{7}$$

Where

K_1 = First acidity constant for protolysis of H_2CO_3 (Strumm and Morgan, 1996). It is $10^{-6.46}$ for 10°C and ionic strength of 0 (Strumm and Morgan, 1996).

Ammonia (NH_3) is calculated from NH_4^+:

$$[NH_3] = \frac{[NH_4^+]}{[H^+]*K} \tag{8}$$

Where

K = Activity coefficient factor is $10^{9.244}$ (NIST, 2004)

Electrons (e^-) are calculated from NH_3:

$$[e^-] = \left(\frac{[NH_3]}{[H^+]*K*[NO_3^-]}\right)^{\frac{1}{8}} \tag{9}$$

Where

K = activity coefficient factor is $10^{109.956}$ (NIST, 2004)

3.4.2 Sediments

Organic carbon, inorganic carbon, calcium carbonate ($CaCO_3$) and organic matter (OM) were determined on dry sediment samples using a LOI technique on a TGA machine. Inorganic carbon contribution (%) was calculated from the weight loss during TGA:

$$C_I = TGA(550°C - 800°C) * \frac{MM_C}{MM_{CO_2}} \quad (10)$$

Where

C_I = Inorganic carbon (C) (%)

TGA(550°C – 800°C) = Weight loss due to carbon dioxide (CO_2) removal (%) between 550°C – 800°C

MM_C = molar mass of C; 12.00 g/mol.

MM_{CO_2} = molar mass of CO_2; 44.00 g/mol.

$CaCO_3$ (%) was calculated as the weight loss during TGA:

$$CaCO_3 = TGA(550°C - 800°C) * \frac{MM_{CaCO_3}}{MM_{CO_2}} \quad (11)$$

Where

$CaCO_3$ = Calcium carbonate (%)

MM_{CaCO_3} = molar mass of $CaCO_3$; 100.08 g/mol

Organic matter content was determined by summing the weight loss percent between 105°C - 450°C and 450°C - 550°C:

$$OM = TGA450 + TGA550 \quad (12)$$

Where

OM = Organic matter in dry matter (%)

TGA450 = Weight loss at 105°C - 450°C (%) of dry matter

TGA550 = Weight loss at 450°C - 550°C (%) of dry matter

Organic C roughly represents 50% of OM content. It was calculated by subtracting inorganic C from total C:

$$C_O = C_T - C_I \quad (13)$$

Where

C_O = Organic C (%)

C_T = Total C (%)

Moisture content % (w/w) and dry matter content % (w/w) were determined by mass differences before and after freeze drying:

$$M_w = M_T - M_D \quad (14)$$

Where

M_w = Mass of porewater in sample (g)

M_T = Mass of total wet sediment (g)

M_D = Mass of dry sediment (g)

C_m = Moisture content % (w/w)

C_d = Dry matter content % (w/w)

And

$$C_m = \frac{M_w}{M_T} * 100\% \quad (15)$$

Or

$$C_d = \frac{M_D}{M_T} * 100\% \quad (16)$$

A clear trend between organic matter and dry matter content was observed in several sample tubes that had not experienced cracking. For this reason, a power fit ($y = 167.12x^{-0.714}$, $R^2 = 0.8027$) was applied to the OM against dry matter trend and used to calculate dry matter content for the remaining samples (Figure 15).

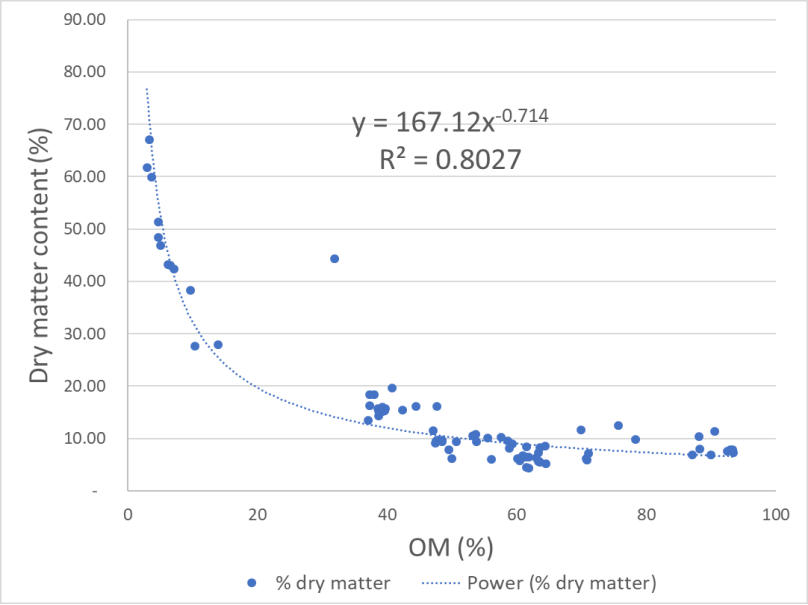

Figure 15: *Power fit curve showing a strong relationship between dry matter and OM content. The curve has been used to calculate C_d for iron storage calculations (see: 3.5 Iron storage calculation). The outliar at (~35%, 45%) is from a BM core.*

3.4.3 Equilibrium calculations

Porewater saturation indexes were calculated for several minerals using CHEAQS Next Version 2019.1 (Verweij, 2005) using the integrated database containing the National Institute of Standards and Technology database version 8.0 (NIST, 2004). Included data is provided in table 5. Program settings were set or had the following:

- Calculations made at 25°C[7].
- Solids were not allowed to precipitate and recalculate.
- Redox equilibria were not included in calculations.
- H+ free activity was used to calculate ionic strength.
- CO_3 free activity was used to calculate ionic strength.
- Ionic strength for other species was calculated within the program based on the attraction and repulsion activity of other species.
- The Davies equation is used to calculate individual ion activity coefficients.
- Sulfide was not included as no sulfide data was present.

Table 5: *CHEAQs inputs used for saturation index determination in all cores. See more 4.1.1.1.*

CHEAQs inputs		
H^+	Ca	Mg
F	Br	NO_3
SO_4	Fe(II)	Fe(III)
PO_4	NH_3	e^-
Mn(II)	Na	Cl

3.4.4 Iron storage calculation

Recovery of iron treatments was calculated using the sedimentary iron concentration and expanded to the whole lake. The following assumptions are made:

- Background iron concentrations will be preferentially taken from literature concentrations before treatment (Table 3). If literature values are not available values will be determined by the minimum concentration in a core layer. Litterature values were found for all treated lakes except Nannewijd[8].
- Some dry matter % (w/w) concentrations were calculated based on the relationship with organic matter (Figure 15).
- Treatment of a core layer was determined based on the layer concentration being above background concentration.
- Treatment layers of a core ends once background iron concentrations are realized or until layer concentrations do not deviate and are visiblibly vertical when compared to treatment layers.

The core Fe concentration was determined with the following calculation:

[7] Temperature corrections were not possible.

[8] Low sediment Fe was found at NW-P between 34 cm – 38 cm and are used as a natural background iron concentration. Based on the reported sediment background Fe concentration and downcore Fe concentration in other iron treated lakes, this value is interpreted as reasonably accurate.

$$Fe_a = (\overline{Fe_T} - Fe_B) * \rho_d * (\frac{\overline{C_d}}{100}) * (L) \quad (17)$$

Where

Fe_a = Recovered treatment iron in the core (g/m^2)

$\overline{Fe_T}$ = Average treatment iron (g/kg)

Fe_B = Background iron (g/kg)

ρ_d = Density of dry matter (kg/m^3)

$\overline{C_d}$ = Average dry matter content (%) (w/w)

L = Treated layer depth (m)

This core value was then expanded to the entire lake:

$$Fe_L = (Fe_P * B_P) + (Fe_M * B_M) \quad (18)$$

Where

Fe_P = South-West core treatment iron (g/m^2)

Fe_M = Middle core treatment iron (g/m^2)

B_P = South-West core contribution to total lake Fe (decimal proportion)

B_M = Middle core contribution to total lake Fe (decimal proportion)

Fe_L = Average recovered treatment iron for the lake (g/m^2)

Thus, recovered treatment iron was compared to the reported iron treatments:

$$R = \left(\frac{Fe_L}{A}\right) * 100\% \quad (19)$$

Where

R = Recovered average treatment iron for the lake (%)

A = Reported added treatment iron (g/m^2)

4. Results

Henceforth, all surface and porewater data will be referred to as 'water' (unless otherwise specified). Referencing a lake as an abbreviation describes a shared profile trait between both cores (Table 6).

Table 6: *Lake abbreviations. Use of abbreviations indicates a shared profile trait between shore-ward and middle cores.*

Lake	Abbreviation
Gravenkoop	GK
Groot Vogelenzang	GV
Sloene	SL
Vuntus	VT
Terra Nova	TN
Botmeer	BM
NW	NW

4.1 Data reliability

4.1.1 Surface and Porewaters

IC vials were not filled to the brim for the Loosdrecht lake complex and Friesland lakes samples. High NO_3^- concentrations determined by IC were recorded in the porewaters of Loosdrecht lake complex cores TN-M, VT-P, and VT-M as well as Friesland lakes cores NW-P, NW-M, BM-P, and BM-M. IC analysis was run twice by different technicians on the Loosdrecht lake complex samples and returned similar results. The source of the elevated concentrations is interpreted as being a dilution error or an error in data reporting.

Data reporting for SL-M pH, alkalinity, ICP-OES, IC, and spectrophotometric measurement data revealed a potential mismatch of the 5 cm and 6 cm data points with the profile trends and were moved to the 1 cm and 2 cm data points respectively; the original 1 cm, 2 cm, 3 cm, and 4 cm data points were shifted down. This has been attributed as a field sampling and labeling error.

Porewater pH at the 1 cm depth differed greatly from surface water values. This has been attributed to the lack of temperature correction on the device. The difference between the surface water pH and 1 cm pH data point has been added to all porewater pH.

Reeuwijk and Loosdrecht lake complex porewater ICP-OES analysis was determined using a seawater analysis method. The surface waters were analyzed using a freshwater method. No corrections have been made to this dataset. Friesland lakes were not affected.

Unexpectedly, Fe^{3+} was recorded in the porewaters near the core termini for all treated lakes. This presence could be due to aerobic handling; however solid particles were not visible in the filtered porewater samples. Porewaters were quickly acidified after sampling.

4.1.1.1 Data validation

Literature values were obtained through publications in scientific journals and technical reports. Several technical reports were translated from Dutch to English using Google based translation (2018 version). The overall translation was useful to gather background information, however certain aspects may have been lost in translation. Effort was made to confirm obtained data through water manager interviews.

Due to overlap of water phase total Fe determined by ICP-OES and Ferrozine method indicate that iron concentrations obtained through both methods represents accurate porewater recovery (Appendix 3: Data files. Likewise, phosphate from the ascorbic acid method and ICP-OES total P overlap. This suggests total porewater P predominantly phosphate. Total S and sulphate from ICP-OES and IC show similar quantity in porewater profiles (shift in ICP-OES surface to 1 cm porewater due to different method use for Reeuwijk and Loosdrecht). Alkalinity in the surface water from the Gran titration method and 1 cm

porewater from the bromophenol blue method contain close values, thus they indicate practical representation of alkalinity values. Total ICP-OES Ca and Mn indicated as representative as they do not show deviation between surface and porewater measurements, nor do metals Fe, Ca, and Mn appear to be affected by the different analysis methods.

Saturation indices (SI) returned from CHEAQs show logical oversaturation with respect to Fe and P phases and are interpreted as being useful despite not containing S^{2-} data (Figure 16). Fe(III) or Fe(II) data was included for calculation if the ferrozine method determination returned positive concentrations (several lakes had Fe(III) and Fe(II) concentrations below the detection limit). Negative results of other inputs were also excluded from calculation. The saturation index for $Fe_2^{3+}O_3$ is interpreted as representing the α-phase iron(III) oxide mineral hematite due to the environment's pH, temperature and presence in an aquatic environment.

The surface and porewater profiles in the results and discussion section reflect spectrophotometric determination of the Ferrozine method (Fe(II) and Fe(III)), ascorbic acid determination of phosphate, alkalinity (porewater only), and ammonium. ICP-OES results are shown for total Ca and total Mn while IC results for sulphate and nitrate are plotted. Note that surface waters (-2 cm depth) were sampled by boat and filtered with a 0.2 µm new disposable syringe filter while porewaters were sampled with a 0.15 µm rhizon.

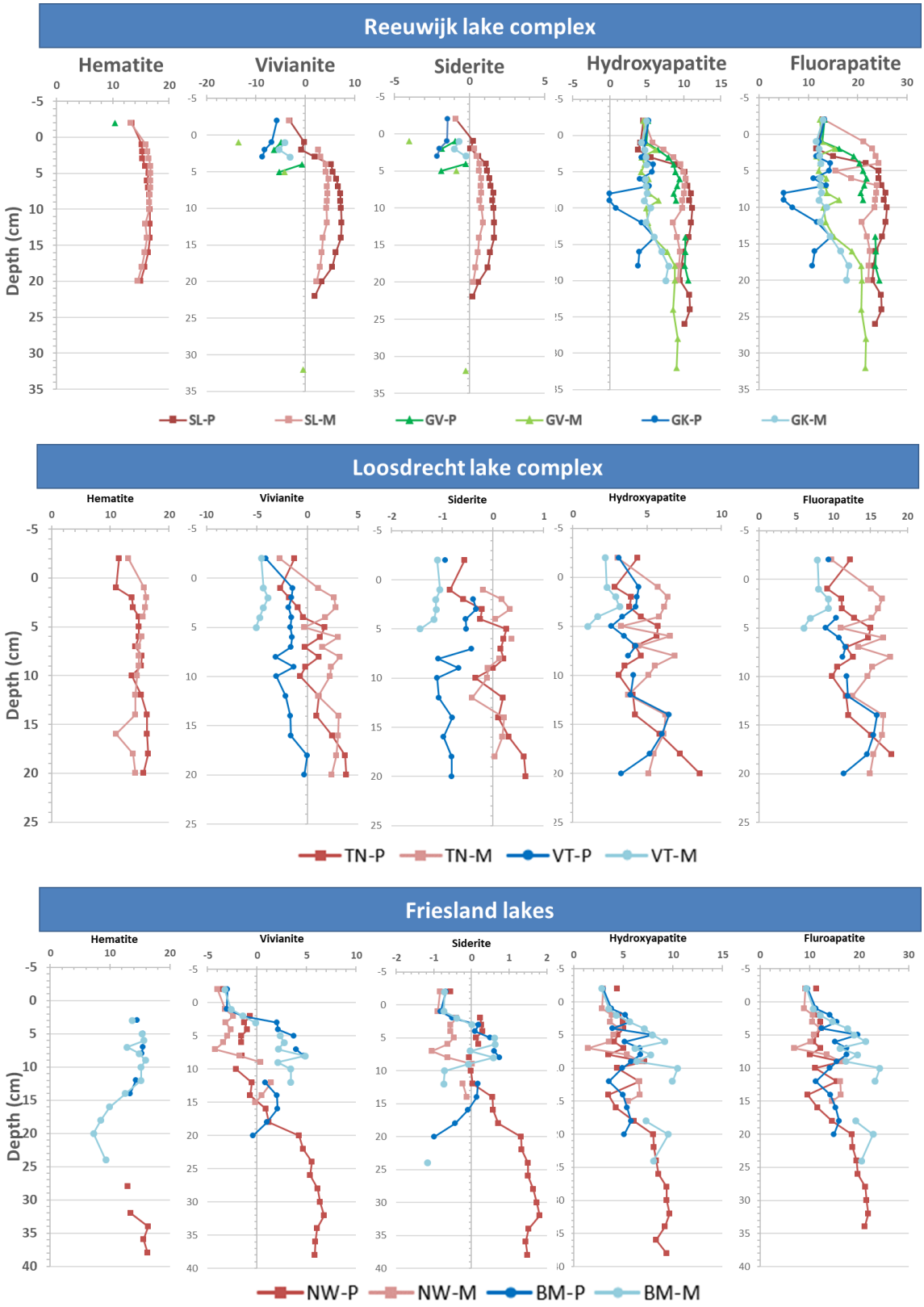

Figure 16: *Saturation index profiles for hematite ($Fe_2^{3+}O_3$), vivianite ($Fe_3^{2+}(PO_4)_2 \bullet 8H_2O$), siderite ($Fe^{2+}CO_3$), hydroxyapatite ($Ca_5(PO_4)_3(OH)$), and fluorapatite ($Ca_{10}(PO_4)_6F_2$) in the respective cores. Note legend at bottom of each lake system. Note surface waters (-2 cm depth) were sampled by boat and filtered with a 0.2 µm new disposable syringe filter while porewaters were sampled with a 0.15 µm rhizon. A -2 cm depth indicates a surface water value.*

4.1.2 Sediments

Due to sediment consolidation in several cores, correction for consolidation was made according to table 3. During core slicing of TN-M the core pushing tool became stuck and broke. After the break the remaining sediments were extracted with smaller diameter tool. The break is due to variation of the inner diameter of the Plexiglas tube.

During replacement of a cracked Greiner vial the GK-M 20 cm sample was replaced and labeled GV-M 20 cm; the original cap was secured to the new incorrectly labeled vial. All sediment analyses were affected; raw data files have not been altered. This error was realized following the two separate CN analysis runs, each recording one GV-M 20 cm sample and an absence of the GK-M 20 cm sample. Using the CN result trend and the originally labeled cap I corrected the data during sediment data treatment.

XRF-P analysis reveals that VT-M and NW-M contain a large amount of silica sand.

Silicon dioxide (SiO_2) was added in order to achieve desired weight for TGA, XRF-P and CS analysis. Results were corrected by the technician using the sample weight in proportion to silicon dioxide weight (specific samples are available in the appendix 3: Data files). Most corrected samples are trusted while the TN-M and TN-P 3 cm and 4 cm samples determined by XRF-P and CS analysis are interpreted as errors.

4.1.2.1 Data validation

Sediment profiles for sediments were validated through comparison with OM and proportion of sample weight to SiO_2 weight, the plotted profiles are therefore reliable representations of lake sediment processes. Results which were clear outliers or had low sample weight were removed. Despite screening, TN-M and TN-P 3 cm and 4 cm deviate from profile trends and may indicate potential error. C values obtained through CN and CS analysis indicate a mismatch of data points. Upon calculating organic C for both methods, a common trend is observed in the CN determination but not for the CS determination indicating that total S may not be trustworthy. However most total S data is indicative of useful sediment profile trends and concentration values for interpretation of lake processes with respect to P binding (due to trend similarities with associated elements).

4.2 Surface and porewater chemistry

Water profiles represent aqueous (<0.02 µm; dissolved), nanoparticulate (<0.10 µm), or colloidal (<1.00 µm) phases that can pass through a 0.15 µm rhizon filter (0.20 µm for surface waters) (Figure 3). Surface water parameters measured in the field are reported in appendix 4.

4.2.1 Reeuwijk lake complex

The Reeuwijk lake complex water profiles, PO_4^{3-}/total Fe, and total Fe/PO_4^{3-} ratios are plotted at the end of the section (Figure 17-18). NO_3^- concentrations were highest in SL-P and SL-M. NO_3^- was removed from the surface water to 1 cm or 2 cm of porewater in cores GK-P, GK-M, GV-P, GV-M, and SL-M. However, NO_3^- concentrations in SL-P were sustained to 9 cm below the SWI. Highest total Mn concentrations (of all cores) were observed for SL-P and SL-M; SL-P has a deeper total Mn peak than all other cores.

Fe(III) was not observed within untreated lake cores GK-P and GK-M. High Fe(III) concentrations were present in SL-P and SL-M up to ~20 cm. Fe(II) concentrations minorly increase from the surface water to approximately 4 cm in GK-P, GK-M, GV-P, and GV-M. SL Fe(II) peaks around 12 cm. SL-P Fe(II) increases

between 2 cm and 6 cm at a rate of ~20 µM cm^{-1} while phosphate increases at ~21.6 µM cm^{-1}. SL-M Fe(II) concentrations are about ⅓ of SL-P concentrations while Fe(III) concentrations are similar in both cores. GV Fe(III) or Fe(III) is near 0 µM over the entire core length, however GV-M Fe(II) slightly increases from 24 cm to 32 cm.

Phosphate is near 0 µM for GK. SL phosphate observes similar profile trend as Fe(III). Water total Fe/phosphate ratio is high above ~4 cm in SL whereas high phosphate/total Fe is found for GK and GV towards the SWI. Phosphate, ammonium, and alkalinity observe profile trends that increase over the same interval whereas the sulphate trend is mirrored and decreasing over the same interval. Surface water sulphate for SL, GV, and GK is ~190 µM, ~300 µM and ~ 400 µM; the slope of their concentration decrease is similar. GK-P sulphate decreases more rapidly with depth than the other cores.

4.2.2 Loosdrecht lake complex

Water profiles, PO_4^{3-}/total Fe, and total Fe/PO_4^{3-} ratios are plotted at the end of the section (Figure 19-20). NO_3^- in TN-P decreases from the surface water to the lower limits of detection (~2.3 µM) by 5 cm. Total Mn in VT-P, VT-M, TN-P, and TN-M is similar and highest and peaks between 2 cm and 5 cm. Total Mn has a peak at 5 cm for TN-P and has a valley at 5 cm in TN-M. Fe(III) is near 0 µM for VT. VT-P Fe(II) is observed in the entire core but is near 0 µM in VT-M. TN-P Fe(III) is increasing downcore whereas TN-M Fe(III) is decreasing downcore. Both TN cores show Fe(II) increase with depth.

VT-P PO_4^{3-} slightly increases with depth in the lower sediments whereas VT-M was near 0 µM. There is a high phosphate to total Fe ratio at 16 cm. The TN-P PO_4^{3-} profile resembles the VT-P profile but has a higher concentration below 15 cm. TN-M PO_4^{3-} is the highest in Loosdrecht and dips at 5 cm. A ~9 mol/mol total Fe/phosphate ratio increase is observed for TN-P between 6 cm and ~18 cm. In all cores except VT-M increases and decreases in NH_4^+ and PO_4^{3-} are observed over the same interval for the respective core. Alkalinity is mostly stable with depth for Loosdrecht cores. SO_4^{2-} decreases from the surface water to approximately 20 cm in VT-P. VT-M SO_4^{2-} increases with depth. TN-P SO_4^{2-} concentration is not significantly decreasing between 3 cm and 10 cm.

4.2.3 Friesland lakes

The water profiles, PO_4^{3-}/total Fe, and total Fe/PO_4^{3-} ratios are plotted at the end of the section (Figure 21-22). Total Mn in BM peaks at ~5 cm. NW total Mn is increasing with depth throughout the entirety of both cores. BM Fe(III) is present in water samples between ~3 cm and 14 cm. BM Fe(II) peaks at 8 cm and thereafter decreases towards 0 µM. NW-P Fe(III) spikes at 34 cm and is present for the remainder of the core. NW-P has a localized Fe(II) peak at ~4 cm and increases with depth at a rate of ~9.6 µM Fe(II) cm^{-1} between 18 cm and 32 cm. NW-P PO_4^{3-} increases from 18 cm to 32 cm at a rate of ~5 µM PO_4^{3-} cm^{-1}. Both PO_4^{3-} and Fe(II) decrease with depth after the NW-P ~32 cm peak.

PO_4^{3-}/total Fe ratio spikes for BM at the 20 cm and 24 cm points whereas NW-M spikes at 9 cm and 14 cm. Water total Fe/phosphate ratio is high in NW-P at 2 cm and 14 cm, below 18 cm the ratio is constant. BM-P total Fe/phosphate ratio peaks at 5 cm (also for BM-M) and 12 cm. High surface water BM sulphate concentration is relatively stable to ~10 cm; below 10 cm sulphate decreases towards 0 µM at a rate of ~43 µM cm^{-1}. NW sulphate decreases downcore at a rate of ~17.5 µM cm^{-1} starting from the surface water.

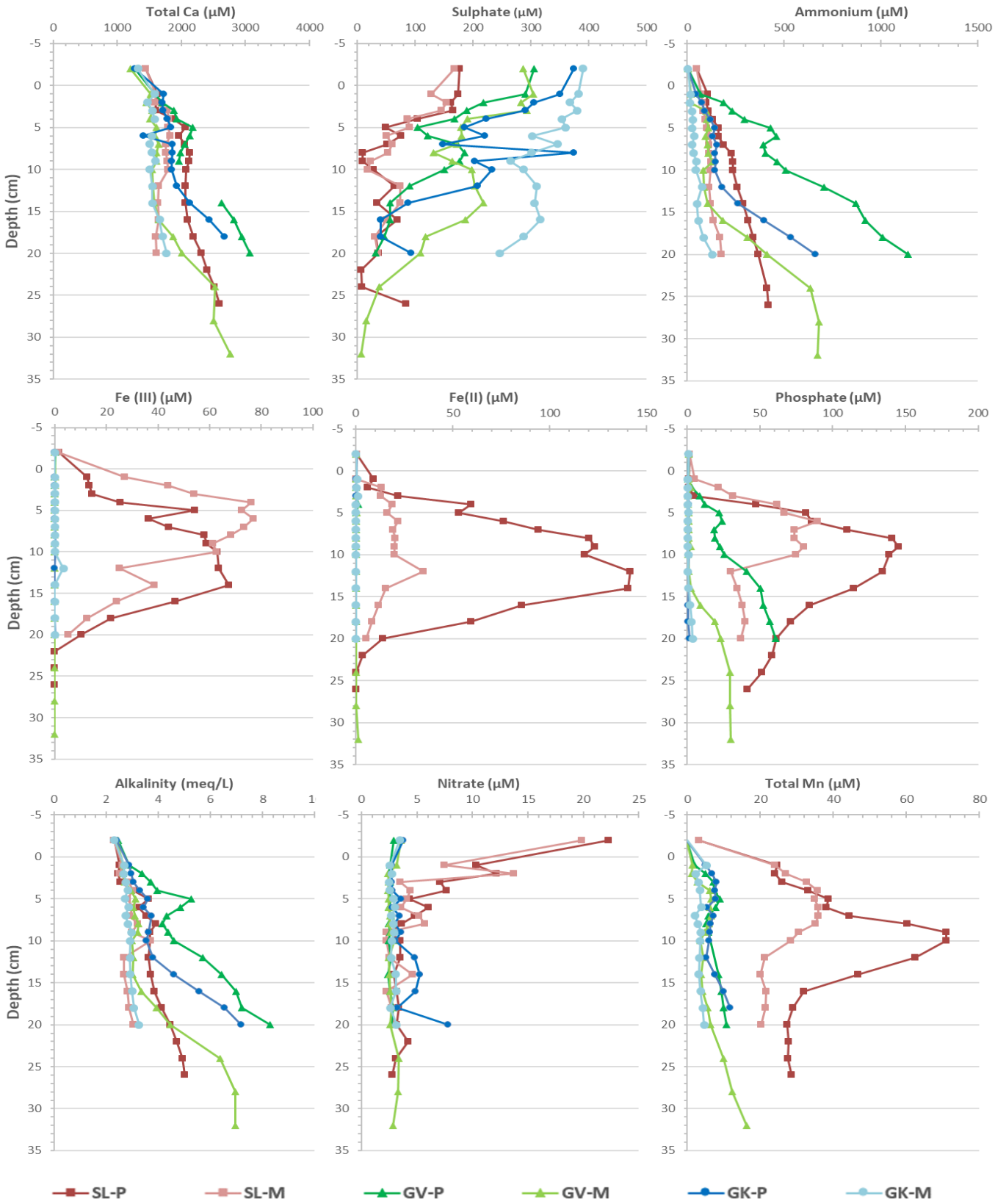

Figure 17: *Reeuwijk lake complex surface and porewater composition. Note the legend at the bottom of the figure. A -2 cm depth indicates a surface water sample. Note surface waters (-2 cm depth) were sampled by boat and filtered with a 0.2 µm new disposable syringe filter,* porewater has been 0.15 µm filtered. *Porewater total Mn and total Ca were determined by a saltwater ICP-OES method.*

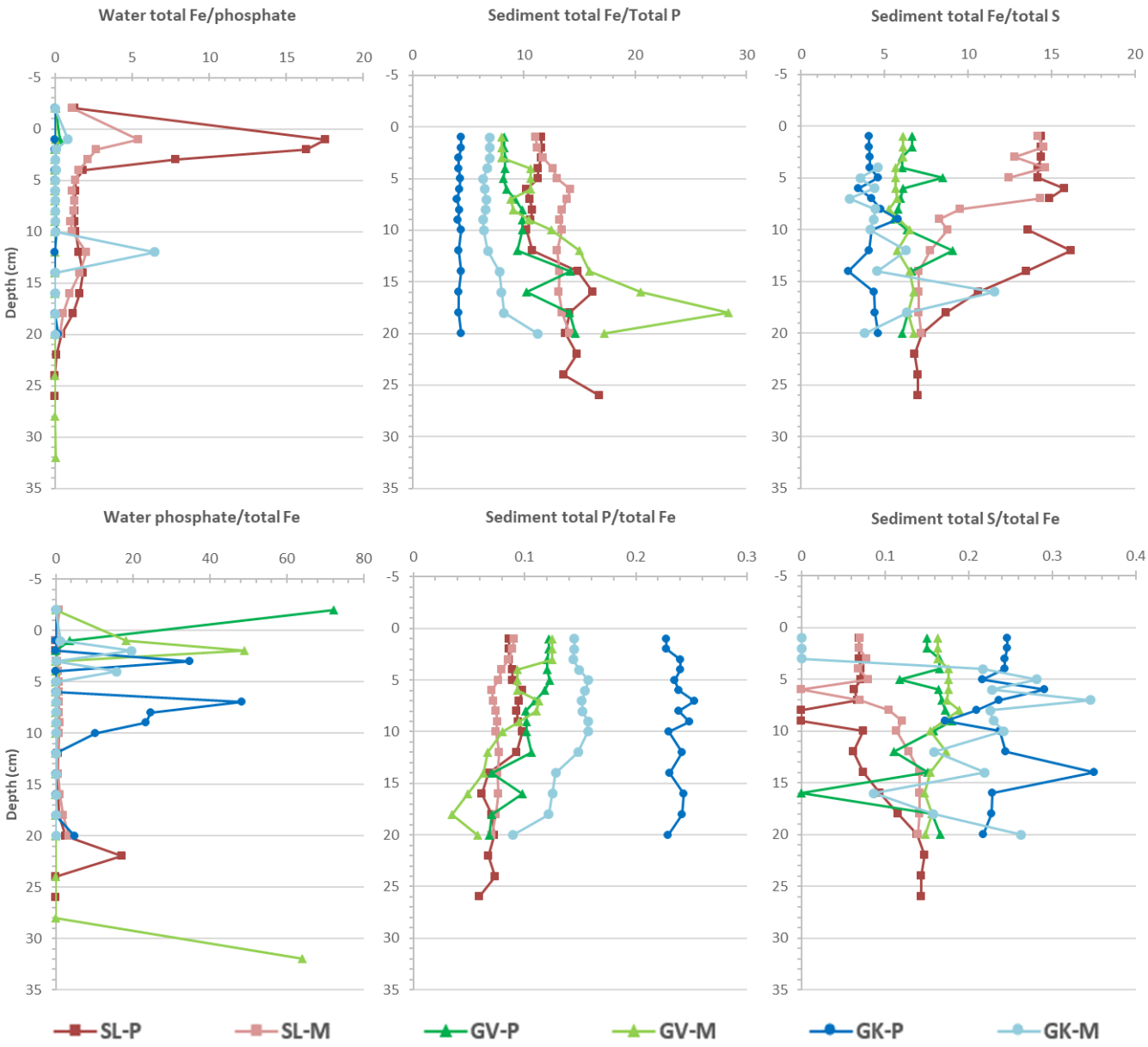

Figure 18: *Reeuwijk total Fe/phosphate, total Fe/total P, and total Fe/total S ratios for the surface and pore waters (left), sediments (middle and right). All ratio profiles given as mol/mol. Note the legend at the bottom of the figure. Note surface waters (-2 cm depth) were sampled by boat and filtered with a 0.2 µm new disposable syringe filter, porewater has been 0.15 µm filtered.* ***Top row ratios*** *are empirically based on laboratory or field studies and have all been suggested as tools indicative of P loading available for water managers while* ***bottom row ratios*** *are empirically based from laboratory or field studies and have been used as indications of specific P or Fe binding minerals in their respective environments (Table 8).*

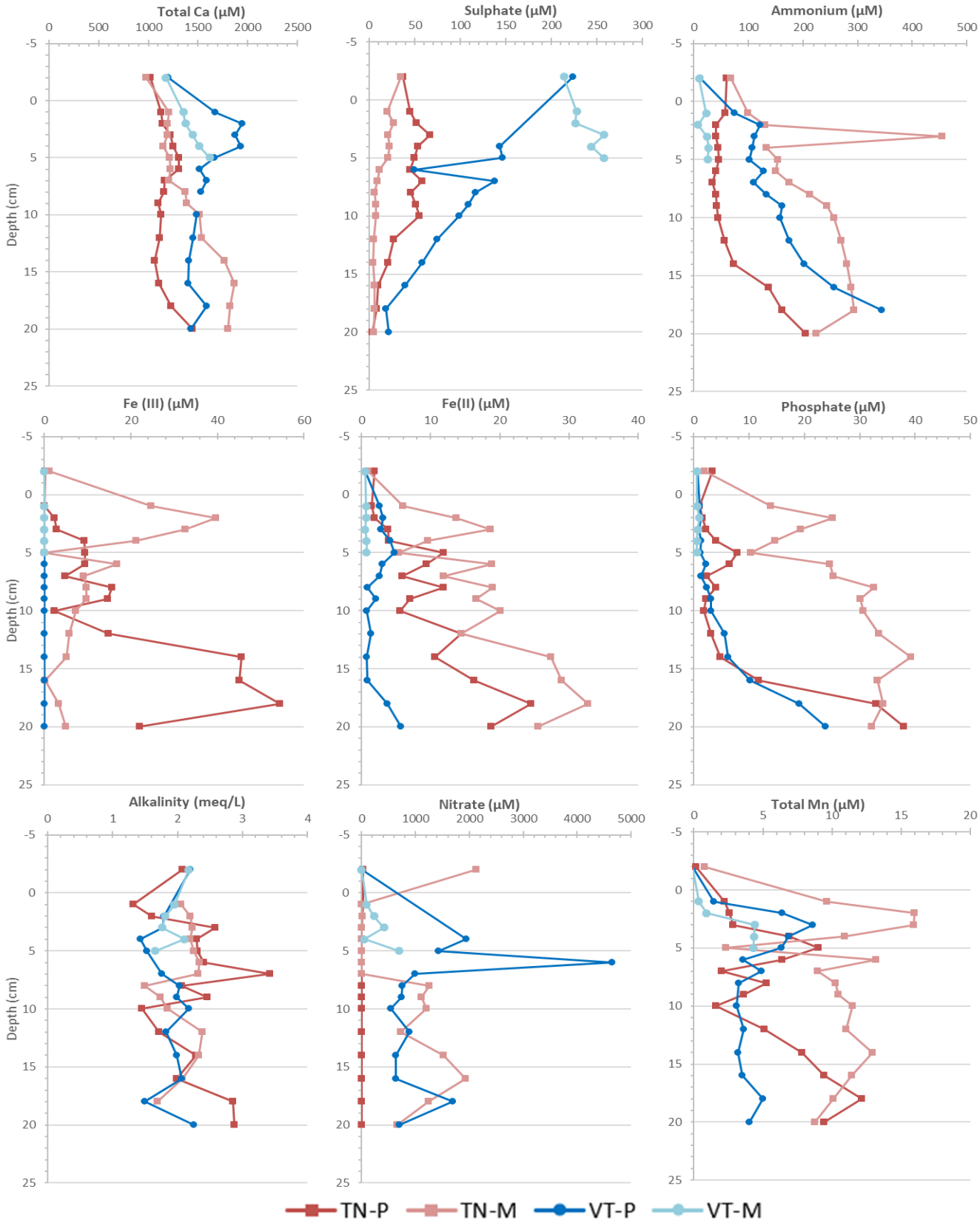

Figure 19: *Loosdrecht lake complex surface and porewater composition. Note the legend at the bottom of the figure. A -2 cm depth indicates a surface water sample. Note surface waters (-2 cm depth) were sampled by boat and filtered with a 0.2 µm new disposable syringe filter,* porewater has been 0.15 µm filtered. *Porewater total Mn and total Ca were determined by a saltwater ICP-OES method.*

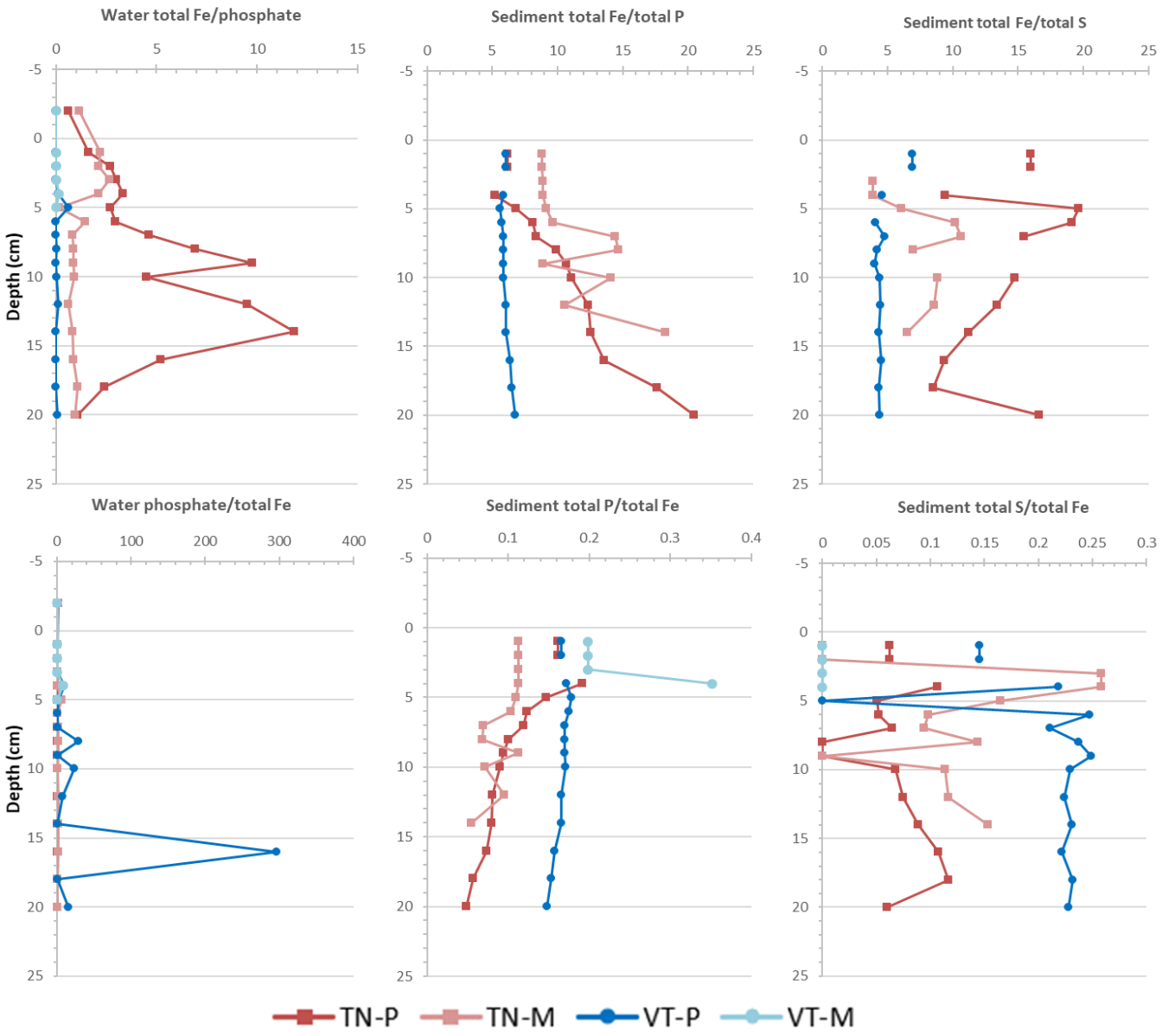

Figure 20: *Loosdrecht total Fe/phosphate, total Fe/total P, and total Fe/total S ratios for the surface and pore waters (left), sediments (middle and right). All ratio profiles given as mol/mol. Note the legend at the bottom of the figure. Note surface waters (-2 cm depth) were sampled by boat and filtered with a 0.2 µm new disposable syringe filter, porewater has been 0.15 µm filtered.* ***Top row ratios*** *are empirically based on laboratory or field studies and have all been suggested as tools indicative of P loading available for water managers while* ***bottom row ratios*** *are empirically based from laboratory or field studies and have been used as indications of specific P or Fe binding minerals in their respective environments (Table 8).*

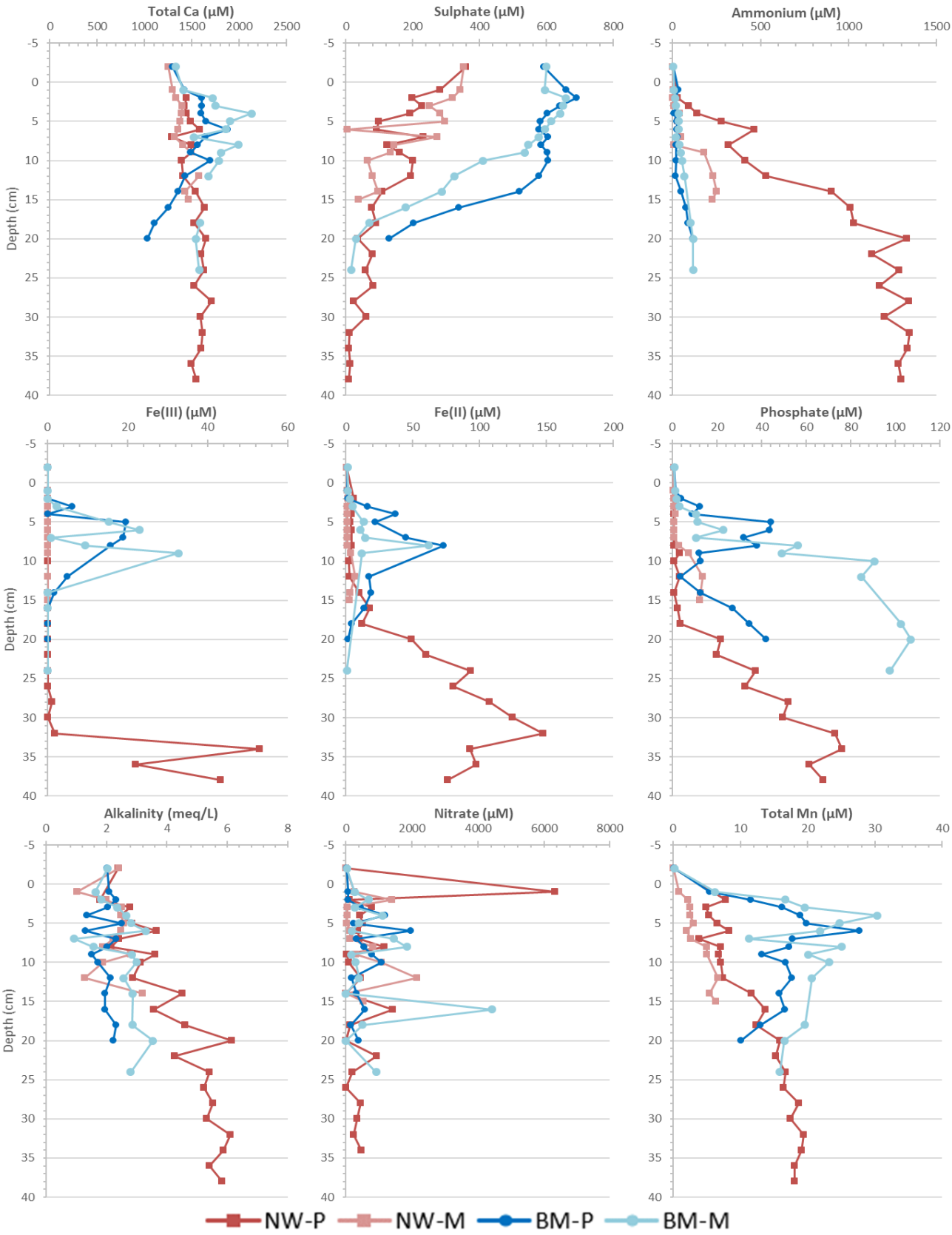

Figure 21: *Friesland lakes surface and porewater composition. Note the legend at the bottom of the figure. A -2 cm depth indicates a surface water sample. Note surface waters (-2 cm depth) were sampled by boat and filtered with a 0.2 µm new disposable syringe filter,* porewater has been 0.15 µm filtered. *Total Mn and total Ca were determined by a freshwater ICP-OES method.*

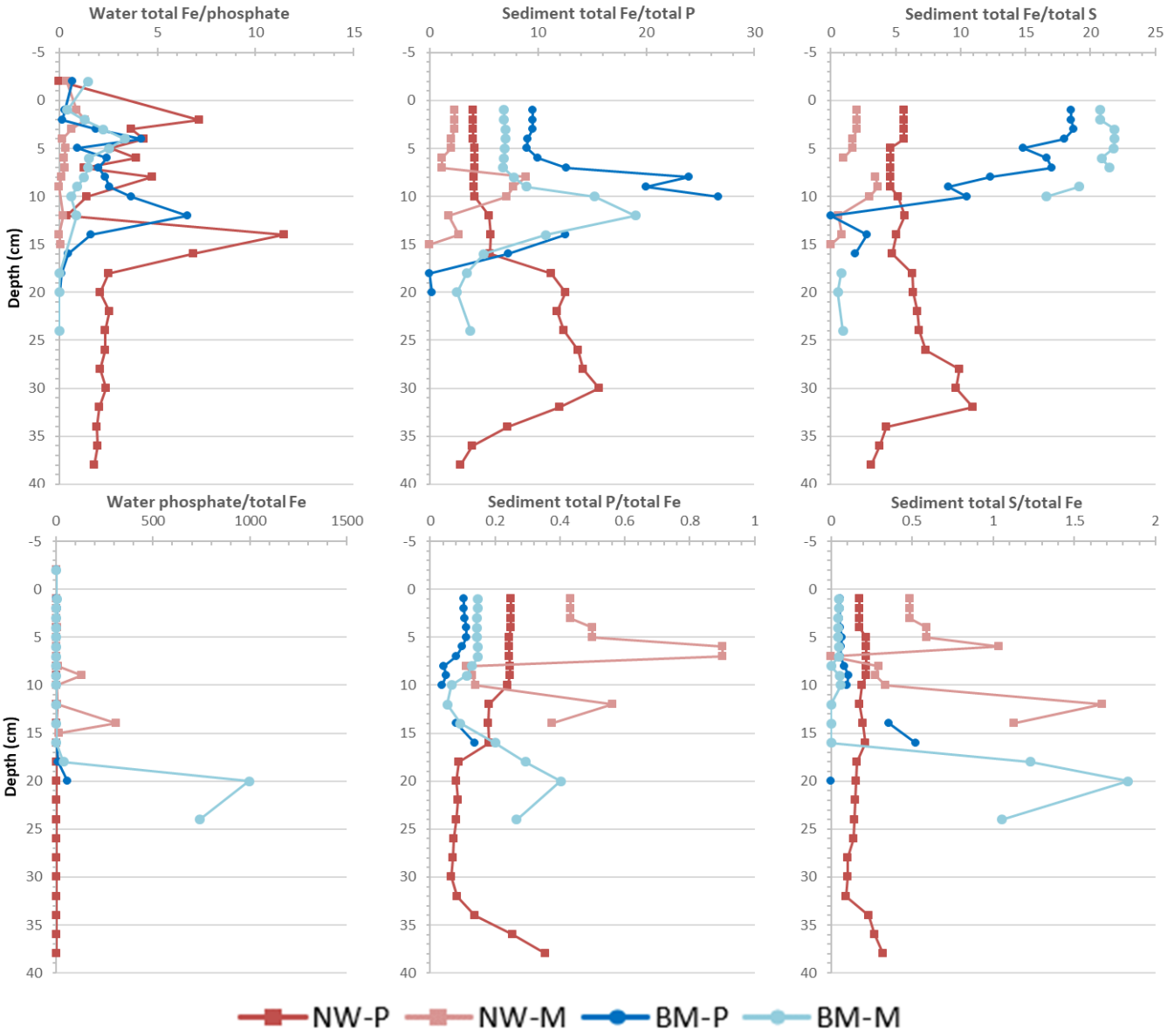

Figure 22: *Friesland total Fe/phosphate, total Fe/total P, and total Fe/total S ratios for the surface and pore waters (left), sediments (middle and right). All ratio profiles given as mol/mol. Note the legend at the bottom of the figure. Note surface waters (-2 cm depth) were sampled by boat and filtered with a 0.2 µm new disposable syringe filter, porewater has been 0.15 µm filtered.* ***Top row ratios*** *are empirically based on laboratory or field studies and have all been suggested as tools indicative of P loading available for water managers while* ***bottom row ratios*** *are empirically based from laboratory or field studies and have been used as indications of specific P or Fe binding minerals in their respective environments (Table 8).*

4.3 Equilibrium calculations

4.3.1 Reeuwijk lake complex

Reeuwijk saturation index (SI) profiles are plotted in figure 16. Where Fe data was available both GK and GV porewaters are undersaturated with respect to vivianite ($Fe(II)_3(PO_4)_2 \bullet 8H_2O$) and siderite ($Fe(II)CO_3$) while highly oversaturated for hematite ($Fe(III)_2O_3$). In both GK and GV hydroxyapatite ($Ca_5(PO_4)_3OH$) and fluorapatite ($Ca_{10}(PO_4)_6F_2$) are oversaturated. SL is highly oversaturated for hematite in the entire core. Both SL vivianite and siderite are oversaturated in most layers, vivianite has a higher SI. SL is oversaturated for hydroxyapatite and significantly oversaturated for fluorapatite.

4.3.2 Loosdrecht lake complex

Loosdrecht saturation index profiles are plotted in figure 16. VT-P and VT-M are respectfully slightly undersaturated for siderite, undersaturated for vivianite, oversaturated for hydroxyapatite and highly oversaturated for fluorapatite. VT hematite SI calculation was not possible. Equilibrium calculations reveal high oversaturation of hematite and fluorapatite, oversaturation of hydroxyapatite, and slight over/undersaturation for vivianite and siderite in both TN-M and TN-P core profiles.

4.3.3 Friesland lakes

Friesland saturation index profiles are plotted in figure 16. Equilibrium calculations show strong oversaturation with respect to hematite and fluorapatite, while oversaturation with respect to hydroxyapatite is determined for BM-P and BM-M. BM-P and BM-M are, with respect to vivianite and siderite, both undersaturated in the upper and lower core while oversaturated towards the middle of the core. Hematite is heavily oversaturated in NW-P at 28 cm and below while hydroxyapatite and fluorapatite (higher SI) are oversaturated over both profiles. Vivianite and siderite are oversaturated in NW-P cores after roughly 14 cm while NW-M is predominantly undersaturated for both minerals.

4.4 Sediment chemistry

4.4.1 Reeuwijk lake complex

Reeuwijk sediment composition profiles are represented at the end of the section (Figure 23) and ratios are plotted in figure 18. OM generally decreases with depth in both GK and GV, whereas SL slightly increases. The slope of GV OM concentration becomes more horizontal after 10 cm.

The GK-P and GK-M cores have relatively stable concentration with depth for total Fe, total P, and total S whereas treatment lakes have larger concentration change with depth. SL-P total Fe and total P are elevated between 6 cm and 12 cm, while total S is lower in this layer compared to deeper sediments. A pronounced increase in SL-P total P is observed between 14 cm to 12 cm and 5 cm to 6 cm. SL-M total Fe increases from ~10 cm to 6 cm which is also observed in total P, while a total S decrease is recorded. In GV increases with depth are seen in both total Fe and total S, however, total P increases over the same interval. Total sediment Fe/total P ratio increases with depth in GV cores and slightly increase in SL cores (Figure 16). Total Fe/total S ratios are relatively constant in GK and GV while the SL-P and SL-M cores are decreasing downcore starting at 14 cm and 7 cm respectively.

4.4.2 Loosdrecht lake complex

Loosdrecht sediment composition profiles are represented at the end of the section (Figure 24) and ratios are plotted in figure 20. Concentrations for VT-P are stable with depth for total Fe, total P, total S,

and OM. VT-M decreases with depth for total Fe, total P, and OM while no data is available for total S. TN-M and TN-P both observe a mostly stable total Fe and OM concentration with depth. TN-P total P decreases with depth. A large TN-P total P and total Fe decrease from 4 cm to 6 cm is likely representative of data errors. TN-P and TN-M total S concentration is elevated at 3 cm and 4 cm and interpreted as data errors; slightly increasing concentrations are observed with depth below 5 cm. TN-M total P concentration is more dynamic below 6 cm. Total Fe/total P ratios are decreasing with depth in both Terra Nova cores whereas the total Fe/total S ratios are higher below 5 cm in TN-M (Figure 16). A highly dynamic letter 'Z' trend is observed in TN-P.

4.4.3 Friesland lakes

Friesland sediment composition profiles are plotted at the end of the section (Figure 25) and ratios are plotted in figure 22. BM cores record a transition zone of 10 cm to ~15 cm in total Fe and OM whereas the total P transition zone is between ~ 6 cm and ~14 cm. BM total S peaks at ~ 9 cm. BM total P/total Fe ratio has a valley at ~12 cm whereas the total Fe/total S ratio decreases after 7 cm.

NW-M is slightly decreasing with depth for total P, total S, and OM whereas a total Fe increase is recorded from 8 cm to 12 cm. NW-P OM, total Fe, total P, total S, total Ca, and total Si all record dynamic concentrations between 10 cm and ~32 cm. Total Fe/total P ratios in NW-P are high between 18 cm and 32 cm whereas NW-M ratios are elevated from 8 cm to 10 cm (Figure 22). NW-P total Fe/total S ratios are relatively stable with depth but are elevated between 28 cm and 32 cm (Figure 22). NW-M total Fe/total S is elevated between 8 cm and 10 cm (Figure 22).

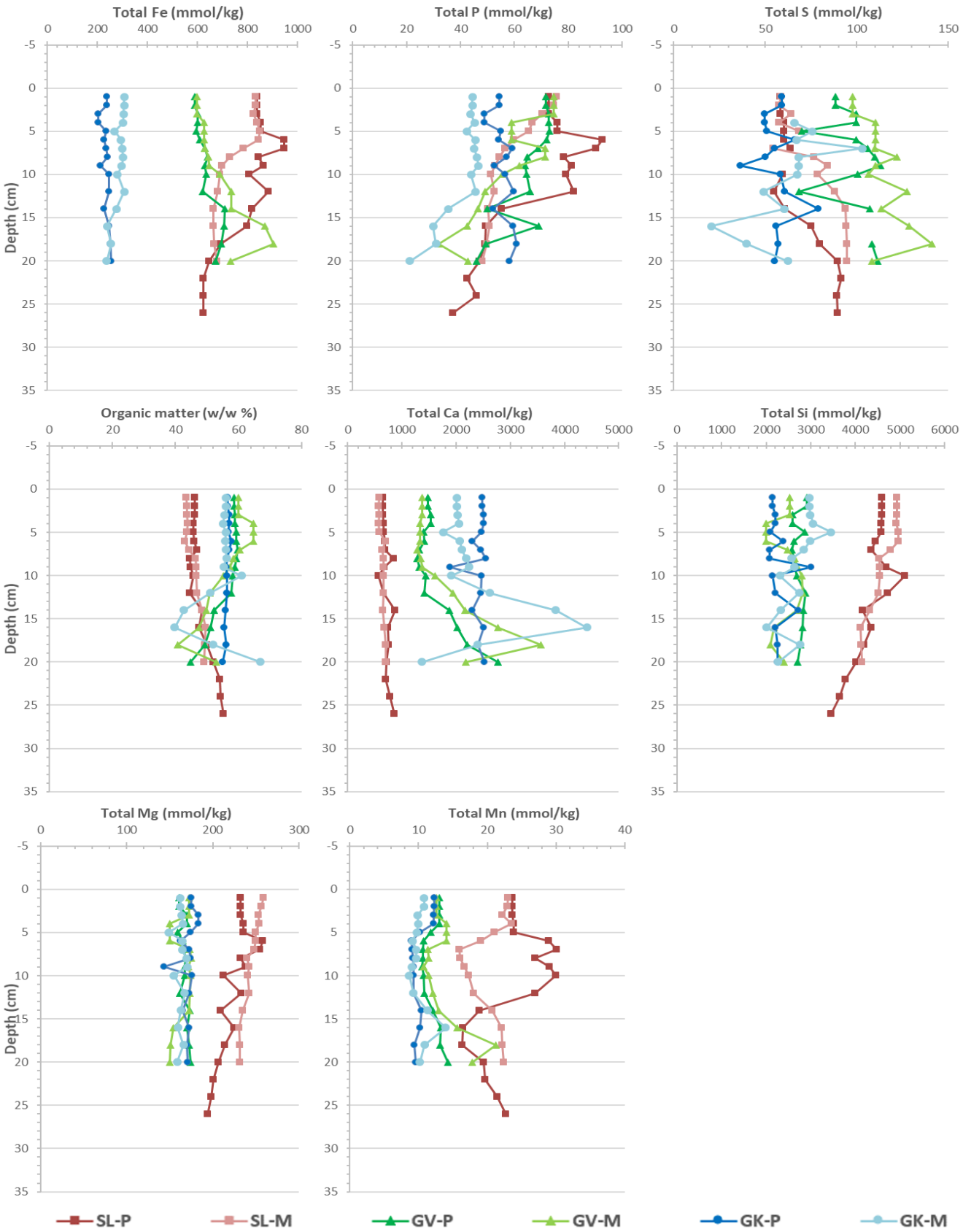

Figure 23: *Reeuwijk lake complex sediment profiles. Concentrations determined from dry matter. Note the legend at the bottom of the figure. Total S was determined using CS while other total concentrations were obtained with XRF-P.*

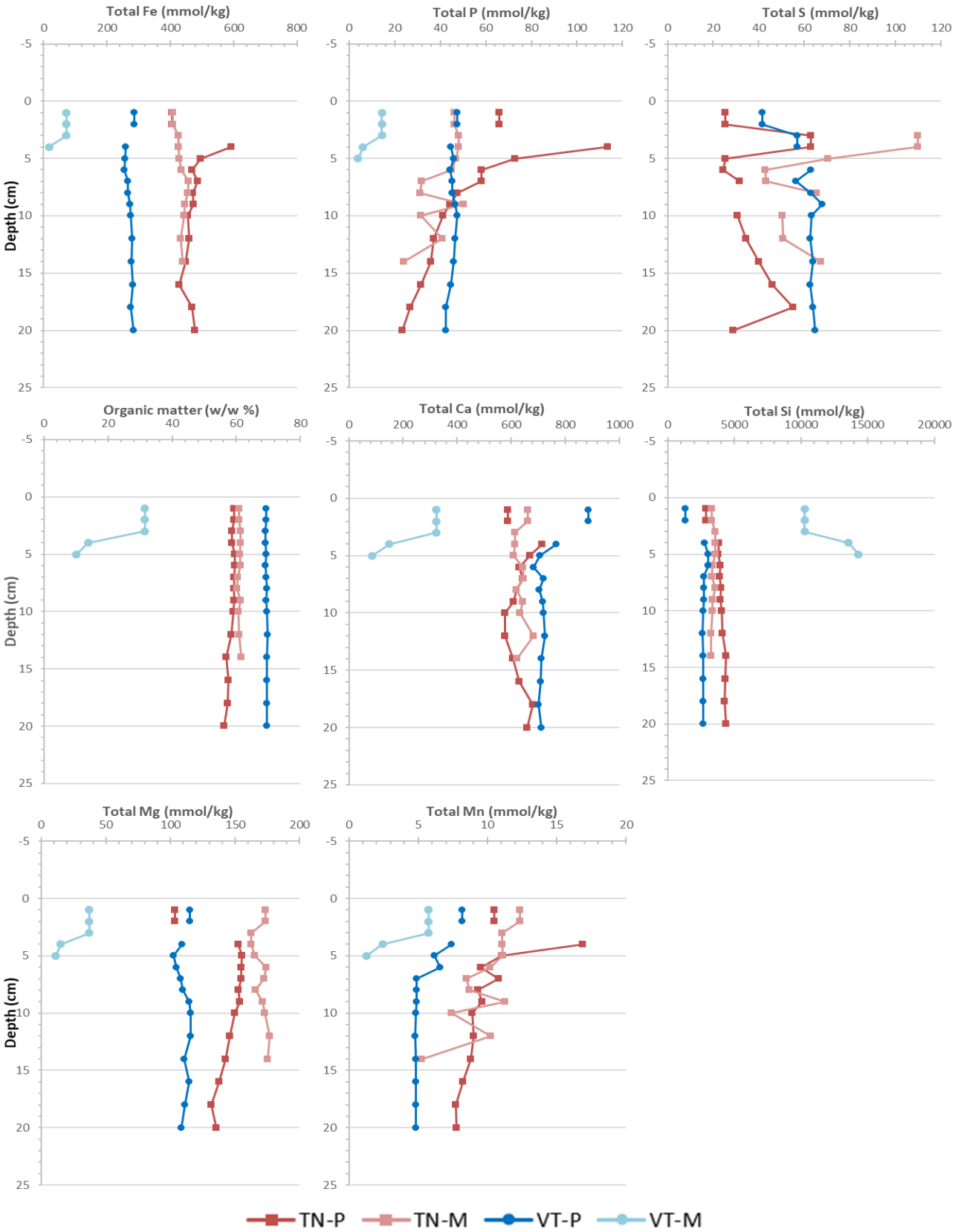

Figure 24: *Loosdrecht lake complex sediment profiles. Concentrations determined from dry matter. Note the legend at the bottom of the figure. Total S was determined using CS while other total concentrations were obtained with XRF-P. Note the TN-P 1 cm and 2 cm total Fe data points are behind the respective TN-M data points and are ~400 mmol Fe/kg.*

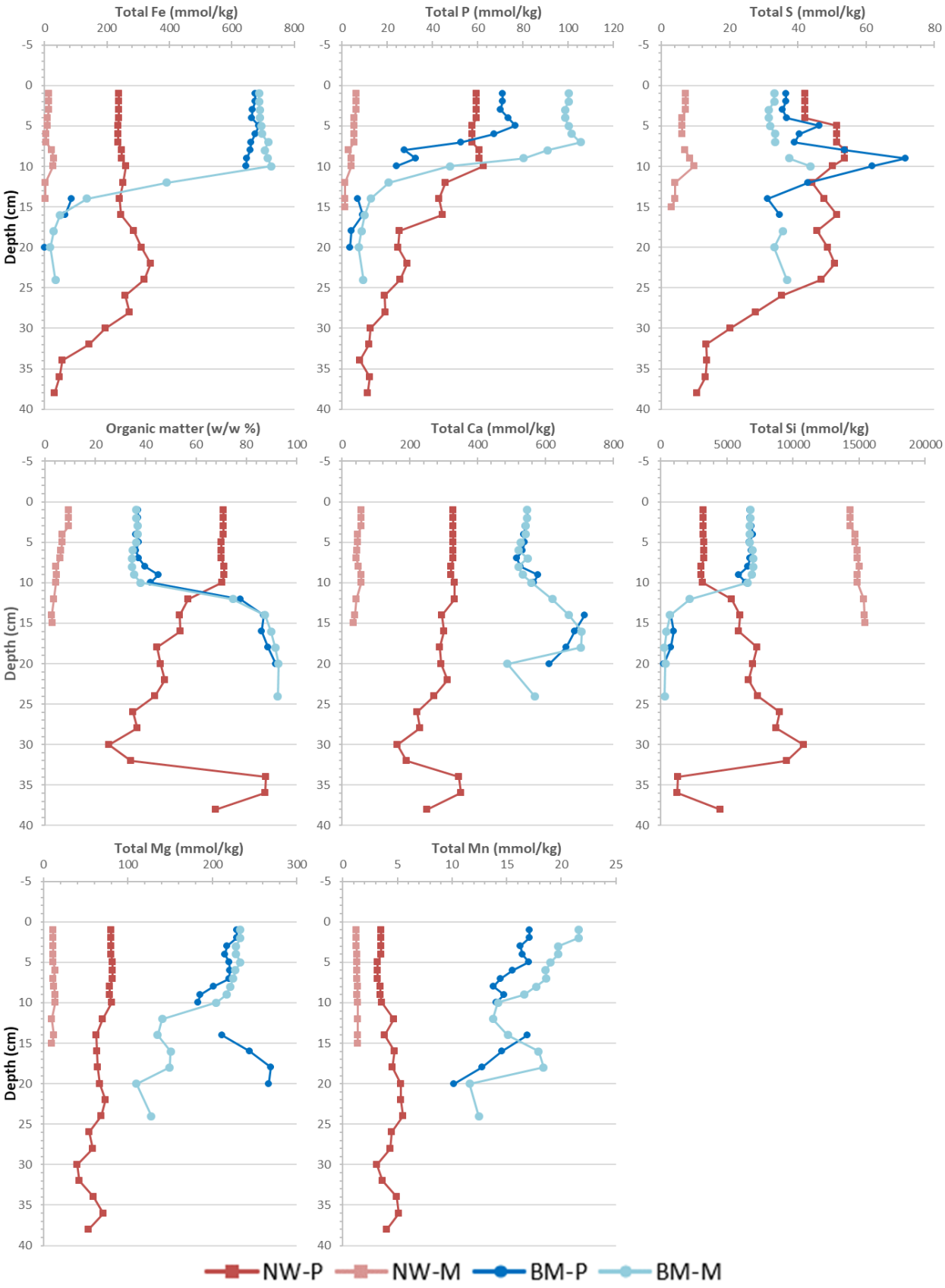

Figure 25: *Friesland lake sediment profiles Concentrations determined from dry matter. Note the legend at the bottom of the figure. Total S was determined using CS while other total concentrations were obtained with XRF-P.*

4.5 Iron treatment visibility and recovery

Iron concentration above reported background content is present in the sediments of every treated lake (Table 3; Figure 26), however NW-M does not surpass background Fe content. Calculated iron treatment recovery using equations 17 – 19 is reported in table 7. The lowest recovery is determined for lake Sloene followed by Terra Nova, Groot Vogelenzang, and Nannewijd respectively. Sediment core Fe was more concentrated in shore-ward cores for NW-P and SL-P whereas GV-M and TN-M recorded similar Fe content (Figure 26).

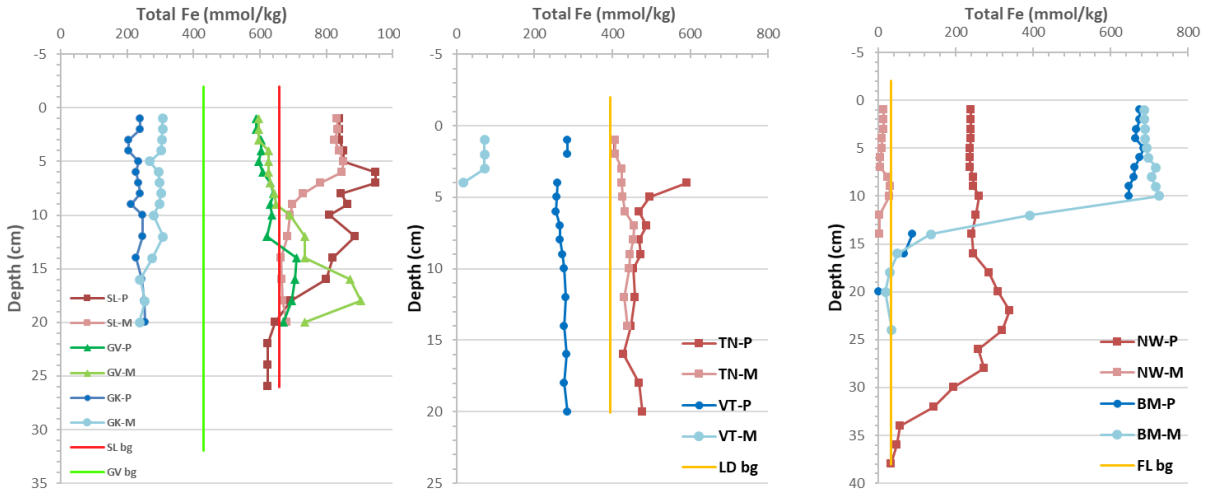

Figure 26: *Sediment total Fe measured from dry mass. Background (bg) concentrations are from literature (table 1) or interpreted below (See: 5.1 Lake iron inventory). Loosdrecht background (LD bg) in indicative of the reported background in both lakes. Friesland background (FL bg) is the proposed background Fe concentration.*

Table 7: *Sediment iron storage calculation. Recovery is calculated from dry matter contents for the noted contribution percent (as a decimal value). Shore-ward (P) core contribution was set low due to the author's understanding that sediment deposition is predominantly directed towards the South-West corner of the sampled lakes (See NW and VT sediment profiles). Note that Nannewijd had a larger iron addition applied to the shore-ward core (table 3). Nannewijd addition is averaged based on different treatment and application areas. Both Sloene and Terra Nova had a wind distributed iron application system whereas Groot Vogelenzang and Nannewijd had manual applications from a boat which were confirmed by a high precision tracking system (table 3).*

Contribution % of P core to total Fe recovery		0.25	
Contribution % of M core to total Fe recovery		0.75	
Lake	**Reported Fe addition (g/m^2)**	**Fe recovered (g/m^2)**	**Fe recovery (%)**
Sloene	178	155.53	87.23
Groot Vogelenzang	100	244.41	244.41
Terra Nova	33	32.87	99.6
Nannewijd	~21.40	113.48	530.29

5. Discussion

5.1 Lake iron inventory

Fe recovery calculation (Equation 17-19) is based on the concentration and contribution of two sediment cores (Figure 26). Background iron concentrations were determined from literature where possible or if literature was unavailable, iron was determined based on minimum core concentration and relation to reference lake iron content (Table 3; Figure 26). Background iron concentration from literature in treated lakes was compared to total Fe content from XRF-P (Table 3; Figure 26). Literature values were within a reasonable range (<~60 mmol Fe/kg dry matter difference) for SL and TN whereas GV sediment Fe content is always above the background. Core terminus NW sedimentary total Fe is below 100 mmol/kg and corresponds well to reference lake BM's downcore iron content, thus NW-P 38 cm is used as the background Fe concentration. For the Reeuwijk and Loosdrecht lake complexes, sedimentary iron in reference lakes GK and VT-P does not match literature or observed background iron. BM iron drastically increases above 10 cm and indicates a significant increase to total iron contribution (and other total element contributions) (Figure 25).

Due to low sedimentary iron in reference lakes GK and VT, these lakes are interpreted as a natural nontreatment reference with a low present day external and internal iron influx (below ~300 mmol/kg) (Figure 23 - 24); this is the result of porewater iron limitation on mineralization (Figure 17, 19). VT-M and NW-M sediment analysis reveals silica dominated sediment type indicative of quartz sand with reduced OM and iron contents (Figure 24-25). As the background iron concentration in treated lake environments is low, concentrations above the background reflect iron addition (Table 3; Figure 26). Therefore, iron addition is recognized as visible in all treated lakes (Figure 26).

5.1.1 Vertical zonation dynamics

TN Fe is mostly constant with depth and is representative of its low iron dosage, drawn out treatment, and slow diffusive transport (Figure 26). TN pore water Fe(II) is similar in both lakes and reflected in a similar relatively constant sedimentary Fe profile shape (Figure 19, 24). Sedimentary iron concentrations are elevated towards the SWI in NW-P, SL-M, and SL-P indicating high surface sediment iron cycling. Additionally, total Fe decrease from 10 cm to 1 cm in GV, 22 cm to 16 cm in NW-P, and 6 cm to 5 cm in SL-P represent decreasing upper core iron in the ferrous wheel as well as a constant Fe burial rate in the recent short term.The rapid GV iron treatment and ~30 years since is reflected by decreasing total Fe content towards the SWI indicating removal of iron from the ferrous wheel. Both SL-M and SL-P increase towards the surface starting at different depths. Total Fe and total S zonation for SL-P and SL-M mirrored about the y axis and represents a high FeS_x as the major Fe binding product (Figure 23); higher SL-P Fe(II) pore water concentrations and deeper Fe(III) reduction zonation is attributed to deeper elevated sedimentary Fe (Figure 23).

5.1.2 Application heterogeneity

Treatment iron recovery calculations indicate lower iron recovery for wind driven dosage systems in SL and TN while higher iron recovery percentages are found in targeted dosing lakes GV and NW (Table 7). This result indicates a potential treatment method influence on recovery calculations and that the iron treatment method may noticeably influence the distribution heterogeneity of treatment iron. Hence, a wind driven distribution system is likely to contain zones of higher and lower treatment iron and therefore P binding capacity. This has been shown in Ter Heerdt et al., 2012, where multiple sediment traps distributed throughout lake Terra Nova recorded Fe treatment recovery between 30% and 70% for

each trap. Highest sediment trap iron recovery was recorded nearest to the treatment platform and generally decreased with distance (Ter Heerdt et al., 2012). This suggests that Fe addition was well dispersed and heterogeneous whereas targeted, GPS ensured treatment, as is the case for GV and NW, is interpreted to be more homogeneous.

The effectiveness of a heterogeneous application is likely to depend on surface water currents, localized surface sediment Fe concentration, localized interal P loading, and the rate of phosphate immobilization processes. Heterogeneous applications may limit localized P binding capacity of the sediments and surface waters by creating Fe deficit zones dictated by sediment settling dynamics. This would ultimately allow pockets of increased bioavailable P flux to accumulate surface water P where a sediment Fe deficit exists, potentially hosting an algae bloom. In this sense, iron oxidation rate and P immobilization rate is important. Results from van der Grift et al. (2014) indicate internally fluxed dissolved Fe(II) may take over a week to be abiotically oxidized and contribute to P immobilization. Summertime Fe(II) oxidation rates were higher (van der Grift et al,. 2014) indicating a control of temperature or pH on Fe(II) oxidation which may increase ferrous wheel cycling and P binding during seasonal climate variations. Similarly, mineralization rates of Fe(III) and Fe(II) minerals are temperature and concentration dependent (Postma, 1981; Curtis et al., 1986). Therefore, internal P trapping should target P release sites to maximize treatment efficiency. Increasing sediment sampling sites would aid in creating an internal P loading map for targeted treatment. Continued research could test this through models Additionally further research is recommended on wind driven iron distribution to bind and prevent internal P loading hotspots, especially regarding water influx zones, the lake parameter, and secluded regions; this research would be advised to test the seasonal P binding capacity. In the meantime, wind driven treatments are recommended to periodically change the position of the treatment platform within the lake as an attempt to increase treatment homogeneity.

Alternatively, high sediment moisture content coupled to a low groundwater table may represent inflow and outflow of groundwater to a lake and its sediments. Thus, overall lower Fe recovery in SL and TN could be more heavily affected by groundwater transport driven dissolved Fe export (Figure 7). It is recommended for continued research to estimate the outflux of dissolved Fe(II) using groundwater inflow over the dissolved iron layer. To a lesser effect, Fe may be removed from the lake systems through hydrological accessibility of water column connections, outputs for water balance, and other anthropogenic needs.

5.2 Redox zonation

The biogeochemical zonation model (Figure 2) is an idealized descriptor of exergonic processes (Table 1) describing OM degradation through biologically mediated chemical processes (Berner 1981b; Froelich et al., 1979). Here the biogeochemical zonation model and the reference lakes will be used as a baseline for discussion. Early degradation and mineralization of organic matter in the sampled lake environments is driven by the same processes that occur in stratified lake and marine systems.

Surface water dissolved oxygen concentration indicates aerobic conditions in the water column (Appendix 4). Expected decreases in O_2 would be due to aerobic respiration. Relatively constant OM content in the upper sediments indicates some oxygen presence up to ~10 cm (Figure 23-25). Decreasing NO_3^- concentrations from the surface to the initial porewater indicates a water column NO_3^- producing process (Figure 17-19). As NO_3^- maximums are observed in the surface water it is understood that nitrification (the oxidation of ammonia to NO_3^-) is occurring in the upper water column followed by

NO_3^- reduction to NH_4^+ or denitrification (NO_3^- => N_2) in the lower water column and upper porewater layers. Similarly, iron treated GV and SL record that NO_3^- is reduced in the surface waters to roughly 5 cm (Figure 17) indicating similar conditions to reference lakes and no significant effect of iron addition on NO_3^- redox zonation which cannot be explained by mixing.

Mn redox zonation is shown in the sediment and porewater total Mn profiles for which there is a representative trend of porewater Mn cycling and mineralization corresponding to sediment profile peaks and valleys in reference lakes GK and BM, but not VT-P (Figure 17-19, 23-26). Elevated SL porewater phosphate between 5 cm and 10 cm corresponds to Fe(III) and porewater total Mn (Figure 17). SL-P and SL-M both feature higher than expected total Mn concentration in the sediments and porewater (Figure 17, 23). Hence SL-P and SL-M high porewater total Mn concentrations between 1 cm and ~16 cm (Figure 17) indicate treatment ferric chloride solution may have included Mn as a biproduct. Alternatively, groundwater flux from lake Broekvelden is possible. Within SL, the total Mn porewater trend is slightly deepened compared to the reference lake, however sediment total Mn peaks and valleys are not significantly changed (Figure 17, 23). Differing sediment total Mn concentration trend is observed in sediments and porewaters of both SL cores which is indicative of mixing layer differences. Elevated porewater total Mn below 12 cm in NW-P is coupled to a relatively constant sedimentary total Mn indicating Mn reduction controlled aqueous manganese(II) sulphide formation and diffusive transport (Figure 21, 25). Porewater total Mn zonation in TN-P and TM-M is not different than its reference lake while sedimentary concentrations are slightly decreasing with depth representing strong Mn cycling towards the SWI (Figure 19, 24).

Under idealized conditions Fe redox zonation occurs below the Mn reduction zone (Figure 2). Near 0 µM Fe^{3+}, and low Fe^{2+} concentrations in reference lakes indicate redox and mineralization zonation occurring between the lower water column and ~4 cm to ~14 cm in the sediments for Gravenbroek and Vuntus respectively following a system representative of figure 4. High porewater Fe^{3+} and Fe^{2+} concentrations are found over significantly larger ranges (for TN-P, TN-M, SL-P and SL-M), a deeper range (NW-P), or hardly present (NW-M, GV-P, and GV-M). Fe^{3+} porewater presence at depth is attributed to a combination of mixing deeping Fe oxization zonation, organic ligand/dissolved organic carbon increasing Fe^{3+} solubility, microbial limitation to iron oxide reduction as a function of surface PO_4^{3-} adsorption, or rate limiting microbial reduction on large Fe concentrations (Sholkovitz and Copland, 1981; Stumm and Morgan, 1996; Borch et al., 2007). Larger and deeper porewater Fe presence is attributed to $FeCl_3$ additions changing redox zonation due to reduceable iron oversaturation and rate limited iron reduction while NW-M and GV porewater Fe is concluded as reduceable iron limitation imposed by Fe deposition/substrate characteristics and exhaustion of treatment iron in the ferrous wheel (Figure 17, 19). Fe redox zonation is therefore interpreted as being significantly affected in treatment lakes.

Slightly decreasing SO_4^{2-} concentrations from the surface to porewaters indicates SO_4^{2-} redox processes occurring in the water column/early porewater layer of most sampled lakes (Figure 17-19). Most porewater SO_4^{2-} concentrations decrease from 1 cm below the SWI downcore indicating reduction processes deviating from the idealized biogeochemical model. This can be due to simultaneous reduction processes (Postma and Jakobsen, 1996), effect of ligands on redox potential (Stumm and Morgan, 1996), or be an artifact of mixing. Within the Reeuwijk lakes and NW-P, higher surface water SO_4^{2-} concentrations contribute to higher downcore SO_4^{2-} concentrations. However, low SO_4^{2-} concentrations in the surface water of TN-P and TN-M are relatively stable for several PW layers

revealing little mixing influence and behavior like the idealized model. Within all lakes except SL and BM microbial respiration using SO_4^{2-} as an electron acceptor appears to be increasing the NH_4^+ and PO_4^{3-} concentration. The depth at which SO_4^{2-} concentrations approach 0 µM does not appear to be influenced by iron additions (Figure 17-19). The rate of sulphate removal with depth for all Reeuwijk lakes and NW is ~15 µM/cm indicating similarity between reference lake GK and treatment lakes. However, TN, VT, and BM suggest local lake history influence on the sulfate reduction rate. As most sampled treatment lakes show a similar sulfate removal rate without any influence on removal depth, it has been concluded that there is no noticeable effect of iron addition on SO_4^{2-} redox zonation.

5.3 Ferrous wheel and long-term P fixation

5.3.1 Idealized ferrous wheel profiles

Efficient iron bound P trapping is achieved by the ferrous wheel process (Figure 4) in the redox zone and long-term P storage as vivianite in anoxic layers (Figure 6). Idealized porewater and sediment profiles for an intact and interrupted ferrous wheel are plotted in figure 27. In the intact ferrous wheel dissolved phosphate in the surface water and oxic porewaters will be adsorbed to the surface of solid phase iron oxides. In anoxic conditions dissolved phosphate will be released from the solid phase primarily due to microbial iron(III) reduction (Figure 27). Upward diffusing $Fe(II)_{(aq)}$ to oxygen containing layers will oxidize to $Fe(III)_{(s)}$ and again form iron oxide solids. Downward $Fe(II)_{(aq)}$ diffusion through anoxic layers results in authigenic vivianite formation (or other minerals). Authigenic vivianite formation will trail FeS_x formation, representing its precipitation following sulfide removal (Equation 1, 3). Simultaneous vivianite and FeS_x formation will occur if $Fe(II)_{(aq)}$ is in surplus with regards to sulfide (Equation 2) (Rothe et al., 2015). Degradation of OM releases dissolved phosphate which can lead to further authigenic vivianite formation or trapping in the ferrous wheel if diffused to the oxic layer (if iron is in excess for P binding). Fe removed through authigenic formation of non-ferrous phosphate minerals would require an import of reactive Fe from the sediments for continued functioning. Rothe et al. (2015) have suggested that Fe addition can be used to account for high surface water $SO_4^{2-}{}_{(aq)}$ and OM influx.

In the interrupted ferrous wheel, influx of degradable organic matter bound P and sulfate limit efficient iron bound P trapping (Figure 27). As OM deposition is high, phosphate release due to OM degradation will exceed the removal of P from the sediment by authigenic mineral formation, resulting in the saturation of the ferrous wheel iron(Figure 27). Nevertheless, porewater phosphate increase due to reductive release from $iron(III)_{(s)}$ is also represented (Figure 27). $Fe(II)_{(aq)}$ concentration is lower in the interrupted situation as decreased upward $Fe(II)_{(aq)}$ flux limits oxidizable iron pool (and thus oxic zone phosphate adsorption sites). Limited oxic layer $iron(III)_{(s)}$ represents the interruption of the ferrous wheel is denoted as a unchanging low sedimentary iron concentration from oxic to anoxic layers (Figure 27). Increasing surface water sulphate concentration will result in deepening of the sulfide presence due to rate limiting sulfate reduction. Downward diffusing dissolved $Fe(II)_{(aq)}$ will be exhausted predominantly by authigenic FeS_x formation increasing solid phase iron and sulfur in the anoxic layer.

5.3.2 Ferrous wheel remediation and vivianite formation

Ferrous wheel functioning was identified in lakes if their porewater and sediment profiles were representative of the intact ferrous wheel, significantly contributed to sedimentary P fixation towards the SWI, and contained layers of high surface water to 10 cm $Fe_{(aq)}/PO_4^{3-}{}_{(aq)}$ ratios (≥3.5 mol/mol) matched to a high $Fe_{(s)}/P_{(s)}$ ratio (≥10.0). (Figure 27). The magnitude of ferrous wheel functioning appears to be directly related to iron addition, treatment quantity, and duration since treatment.

Locations of likely vivianite formation are suggested based on the combination of an intact ferrous wheel functioning, $S_{(s)}$/ $Fe_{(s)}$ ratio (<1.1) and matched to a high $Fe_{(aq)}/PO_4^{3-}{}_{(aq)}$ ratio (>3.5). Zonation of hypothesized vivianite presence is suggested to be influenced by iron addition method, groundwater transport, and surface water $SO_4^{2-}{}_{(aq)}$. OM degradation through $SO_4^{2-}{}_{(aq)}$ reduction directly contributes to $PO_4^{3-}{}_{(aq)}$ release from the sediments and $S^{2-}{}_{(aq)}$ formation in the following lakes. Given the observational data, the intact and interrupted ferrous wheel profiles combined with molar ratios are practical indicators of the drivers affecting ferrous wheel functioning, and possible vivianite containing layers.

5.3.2.1 Reference lakes Gravenbroek (GK) Vuntus (VT), and Botmeer (BM)

Similarities to the interrupted ferrous wheel are found within the GK and VT reference lakes (Figure 17, 19, 23-24, and 27). VT porewater and sediment profiles match the 6 idealized interrupted profiles while only 3 of 6 profiles were match for GK (matched profiles are $SO_4^{2-}{}_{(aq)}$, $Fe_{(s)}$, and $P_{(s)}$). High $SO_4^{2-}{}_{(aq)}$ concentrations in GK with a ~15 µM cm^{-1} removal rate indicates a high probability of $S^{2-}{}_{(aq)}$ presence to >25 cm (Figure 17). VT-P $SO_4^{2-}{}_{(aq)}$ removal rate with depth of ~10 µM cm^{-1} indicate likely $S^{2-}{}_{(aq)}$ (Figure 19). This combined with empirically derived porewater and sediment ratios suggests P dynamics (Table 8). Both VT and GK have $Fe_{(s)}/P_{(s)}$ and $Fe_{(aq)}/PO_4^{3-}{}_{(aq)}$ ratios near 5 and 0 respectively suggesting $S^{2-}{}_{(aq)}$ binds $Fe(II)_{(aq)}$ and $Fe(II)_{(aq)}$ is insufficient to bind $PO_4^{3-}{}_{(aq)}$, thus $PO_4^{3-}{}_{(aq)}$ is not being trapped by iron (Figure 18 and 20; Table 8). The likelihood of $S^{2-}{}_{(aq)}$ suggests $FeS_{x(aq)}$ presence while SI calculations indicate vivianite is undersaturated and likely not contributing to noticeable P fixation (Figure 16); however, hydroxyapatite or fluorapatite are suggested as main $PO_4^{3-}{}_{(aq)}$ fixing minerals below the Fe redox zone (Figure 16).

BM presents a situation in which high above background iron concentrations are observed (Figure 25). This is led to a BM match with all 6 profiles of the intact ferrous wheel (Figure 21, 25, and 27). Above 12 cm, $Fe_{(s)}$ is greatly increased and is contributing to the functioning ferrous wheel (represented in the porewater $Fe(III)_{(aq)}$ and $Fe(II)_{(aq)}$ profiles) (Figure 21, 25). Between 12 cm and 14 cm BM $Fe_{(s)}$ concentration plummets (Figure 25); Fe below 14 cm is interpreted as unreactive with respect to reduction and oxidation (Figure 25). Saturation indices indicate high oversaturation with respect to hematite in the entire column and oversaturation with respect to vivianite below ~ 4 cm (Figure 16). However, a ~43 µM cm^{-1} $SO_4^{2-}{}_{(aq)}$ removal rate with depth between 10 cm and 20 cm indicates high probability for $S^{2-}{}_{(aq)}$ diffusing from this zone which (Figure 21). Based on the above points and the $Fe_{(s)}/P_{(s)}$ ratio >~10, vivianite is hypothesized to be present between 8 cm and 15 cm, but is most likely forming and in highest sediment Fe contribution near ~10 cm at a ~4:1 mol $Fe_{(aq)}/PO_4^{3-}{}_{(aq)}$ ratio (Figure 22).

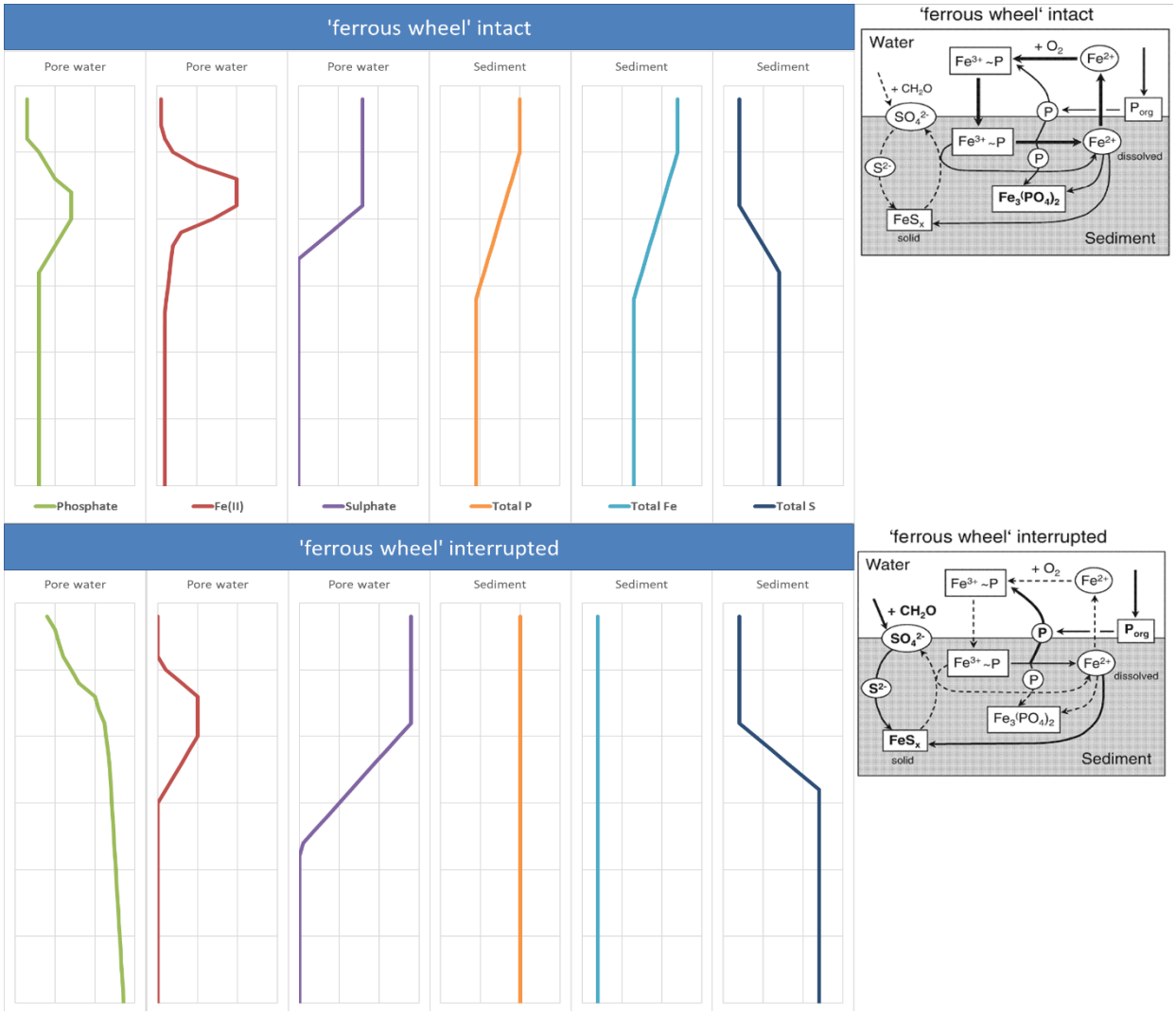

Figure 27: *Idealized profiles for the intact and interrupted ferrous wheel (left). Ferrous wheel schematic from table 6 is shown as a reference (right) (from Kleeberg et al., 2012). The* ***intact ferrous wheel*** *is low in surface water sulphate and OM influx/deposition to the sediments whereas the* ***interrupted ferrous wheel*** *is high in surface water sulphate and OM influx/deposition to the sediments. Further description is provided in section 5.3.1.*

Table 8: *Ratios indicative of P binding processes or phosphate (PO4) release. The same methodology is used here to describe P binding. Smolders et al., 2001, Guerts et al., 2008, and Wang et al. 2018 are based on laboratory or field studies and have all been suggested as tools indicative of P loading available for water managers while other references are empirically based from laboratory or field studies and have been used as indications of specific P or Fe binding minerals and processes in their respective environments (Table 8). The van der Grift et al., 2016 reference indicates table 1 in that publication.*

Ratios					
Phase location	Synthetic solution aeration	Pore water	Sediment		
Ratio	Initial P/Fe	Total Fe/PO4	Total Fe/total P	Total Fe/total S	Total S/Reactive Fe
Ratio units	mol/mol				
Basis	Empirical				
Depth interval	-	~1-10 cm	~1-10 cm	~1-10 cm	Entire column
Value	0.12 - 0.90	~1; 3.5; 3.6	~10; ~30	10	1.1
Ratio (smaller or greater than)	-	Greater	Greated than	Greater than	Smaller than
Ratio indication	specific ratio indicates stoichiometric precipitate	Stop high surface water PO4 concentration or indicate low PO4 flux to SWI	Stop high surface water PO4	PO4 release was supressed	Vivianite presence was favored
Reference	van der Grift et al., 2016 (Table 1)	Smolders et al., 2001; Guerts et al., 2008; Lehtoranta and Heiskanen, 2003	Guerts et al., 2008; Wang et al., 2018	Wang et al., 2018	Rothe et al., 2015

5.3.2.2 Iron treated lakes

Sloene (SL)

SL presents a situation in which iron distribution may be affecting ferrous wheel functioning. SL-M sediment and water profiles observe 6/6 of the intact ferrous wheel profiles while SL-P observes low proportions of $Fe(II)_{(aq)}$ and high $PO_4^{3-}{}_{(aq)}$ and a 4/6 profile match (Figure 17, 23, and 27). However, SL-P $Fe_{(aq)}/PO_4^{3-}{}_{(aq)}$ up to ~ indicates high $PO_4^{3-}{}_{(aq)}$ binding potential which has been attributed to $Fe(III)_{(aq)}$ (Figure 17-18). Both cores recorded $Fe_{(aq)}/PO_4^{3-}{}_{(aq)}$ ratios > 3.5 at 1 cm, yet SL-M decreases below 1 cm to < 3.5 whereas SL-P is > 3.5 to 3 cm (Figure 18). Both cores indicate $Fe_{(s)}/P_{(s)}$ ratios >~10 over their entire length (Figure 18). This leads to my conclusion that there is effective $PO_4^{3-}{}_{(aq)}$ fixation to the sediments, yet separate processes are at play in the two cores.

The cores observe distinct differences in their $Fe_{(s)}$, $S_{(s)}$, and $P_{(s)}$ profiles likely representing localized and distinct sedimentary environments (Figure 23). This in reflected in SL-M where $PO_4^{3-}{}_{(aq)}$ is released with depth between 1 cm and 4 cm at a rate of ~21 µM cm^{-1} while $Fe(III)_{(aq)}$ and $Fe(II)_{(aq)}$ are increasing with depth over the same interval at a rate of ~17 µM cm^{-1} and ~1.5 µM cm^{-1} respectively indicating minimal potential for complete P binding through Fe(III)-P adsorption and Fe(II)-P binding (based on a ~0.7 P:Fe

ratio (vivianite 3Fe:2P ratio) and a 0.6 mol P: mol Fe ratio[9]) (Figure 17). The overall indication is that there is less surplus Fe cycling in SL-M and less long-term P binding potential. This likely due to the lack of increased iron storage (and thus vivianite-based P trapping) in SL-M in the sediments below 10 cm as denoted by mismatch of $Fe_{(s)}$ and $P_{(s)}$ profile (Figure 23).

Two reasons are proposed for this. (1) As porewater sulphate is observed to approach ~0 µM at ~8 cm and be elevated between ~ 10 cm and ~20 cm in both cores it is here hypothesized that groundwater transport is affecting the ~10 cm to ~20 cm sediment layer. Due to a difference between the sediment total Fe and total S profile trends it is suggested that the groundwater flow rate may elevated in SL-M compared to SL-P (Figure 23). Additionally, porewater phosphate concentrations show a pronounced decrease from 10 to 12 cm[10]. (2) Wind driven iron distribution may not be evenly applied (see: 5.1.2 Application heterogeneity). Nevertheless, a SL-M 1 cm porewater total Fe/phosphate ratio indicates current adequate P trapping. Due to the cumulative influences on SL-M, I hypothesize that the ferrous wheel trapping in SL-M will not be sustained throughout all seasons during a given year (summer increased internal P influx) or into the next few years (as sedimentary total S indicates FeS_x mineralization), nor do I suggest the presence of vivianite (Figure 17 and 23).

SL-P porewater Fe/P ratio indicates high P binding capacity between 4 cm and 1 cm (Figure 18). The Fe sediment profile between 6 and 12 cm show a high correlation with $P_{(s)}$ and is indicative of vivianite formation near 15 cm which is supported by the high $Fe(II)_{(aq)}$ and $PO4_{(aq)}$ concentrations and moderate sediment $Fe_{(aq)}/PO_4^{3-}{}_{(aq)}$ and $Fe_{(s)}/S_{(s)}$ ratio of (~2; ~10) (Figure 17-18, 23).

Groot Vogelenzang (GV)

Similarities between the interrupted ferrous wheel and GV are observed for all 6/6 profiles (Figure 17, 23, and 27). $Fe_{(aq)}/PO_4^{3-}{}_{(aq)}$ and $Fe_{(s)}/P_{(s)}$ ratios <1 and < 10 in the upper 10 cm of sediment indicate an interrupted ferrous wheel (Figure 18). The $PO_4^{3-}{}_{(aq)}/Fe_{(aq)}$ ratio above above ~0.5 indicate a lack of P binding to $Fe_{(s)}$ near and at the SWI (Figure 18; based on ratio in streams from Baken et al., 2016). Near 0 µM $Fe(II)_{(aq)}$ and $Fe(III)_{(aq)}$ concentrations indicate a near lack of iron cycling (Figure 17). This is likely due to an exhaustion of the cycling capacity of treatment iron as suggested by increasing $Fe_{(s)}$ with depth and application ~30 years ago (Figure 23; Table 3). Increasing sedimentary Fe and S concentrations with depth coupled to decreasing P suggests a high proportion of FeS_x minerals at below 10 cm and a higher proportion of iron (oxy)hydroxide bound P above 10 cm (figure 12).

Elevated concentrations of $SO_4^{2-}{}_{(aq)}$ are present in GV surface water. The high $S^{2-}{}_{(aq)}$ production has likely led to $FeS_{x(s)}$ binding throughout the column. High OM degradation through $SO_4^{2-}{}_{(aq)}$ reduction is directly contributing to elevated $NH_4^{+}{}_{(aq)}$ and $PO_4^{3-}{}_{(aq)}$ concentrations with depth (Figure 17 and 23). However, $PO_4^{3-}{}_{(aq)}$ is not reaching the surface water which is attributed to fluorapatite and hydroxyapatite mineralization near 5 cm and ~15 cm (Figure 16-17). A $Fe_{(aq)}/PO_4^{3-}{}_{(aq)}$ ratio near 0 indicates vivianite formation is unlikely within this core, yet $Fe(II)_{(aq)}$ at 32 cm indicates a potential for deeper sediment vivianite (Figure 17-18). It is unlikely that vivianite is forming within the sampled sediment column.

[9] Based on results of van der Grift et al., 2016 where Fe(II) oxidation resulted in P/Fe binding ratio of 0.6 mol/mol proposed for groundwater systems with an initial porewater (P/Fe) ratio up to 1.5. This 0.6 mol/mol ratio is used only as an indication of binding efficiency of Fe(III) minerals.

[10] This observation is shown in both ICP-OES and spectrophotometric porewater P and phosphate determinations.

Nannewijd (NW)

NW-P shows indications of an interrupted ferrous wheel in the pore water contents, while indicating intact profiles for $S_{(s)}$ and $P_{(s)}$ (Figure 21, 25, and 27). Low porewater concentrations are sustained in NW-P for $Fe(II)_{(aq)}$ and $PO_4^{3-}{}_{(aq)}$ over the top ~9 cm and lead to a $Fe_{(aq)}/PO_4^{3-}{}_{(aq)}$ ratio > 3.5 for several layers (Figure 22). Meanwhile, the $Fe_{(s)}/P_{(s)}$ ratio is always below 10 for this interval (Figure 22). The total sedimentary Fe deviates from the intact ferrous wheel profile due to the low $Fe(II)_{(aq)}$ and $Fe(III)_{(aq)}$ content (Figure 21, 25, and 27). $SO_4^{2-}{}_{(aq)}$ reduction from the surface 32 cm would produce $S^{2-}{}_{(aq)}$ ultimately limiting Fe mineralization to FeS_x (Figure 21). After 32 cm a ~2 $Fe_{(aq)}/PO_4^{3-}{}_{(aq)}$ ratio indicates a stoichiometric surplus of $Fe_{(aq)}$ for hypothesized authigenic vivianite mineralization and occurrence (Figure 22). This is supported by the increasing $P_{(s)}/ Fe_{(s)}$ ratio below 32cm of ~0.2 and a total S/ Fe ratio of ~0.3 (Figure 22).

Due to a sandy silica substrate the NW-M core the Fe storage potential of the sediment was reduced (Figure 25). The low $PO_4^{3-}{}_{(aq)}$ increase represents OM diffusion from deeper sediment layers. The $Fe(II)_{(aq)}$ concentration is increased by ~7 µM at 12 cm and $PO_4^{3-}{}_{(aq)}$, however high sulphate concentrations will limit permanent P burial (Figure 21 and 25). As a conclusion, low 1 cm to 10 cm $Fe(II)_{(aq)}$ and $Fe(III)_{(aq)}$ indicates Fe cycling is not significantly present in NW (Figure 4 and 21) and therefore interrupted. Increasing NW-P $P_{(s)}/ Fe_{(s)}$ ratio of less than ~0.2 for total P/total Fe indicate unfavorable ratios for vivianite detection, however below 32 cm increasing $P_{(s)}/ Fe_{(s)}$ ratio may indicate vivianite presence. NW-M vivianite formation is not likely due to overlap of the total P/total Fe and total S/total Fe ratios combined with presence of sulphate reducing conditions (Figure 21-22).

Terra Nova (TN)

TN presents a situation in which few profiles match the intact ferrous wheel (only matching $S_{(s)}$ and $P_{(s)}$) and interrupted ferrous wheel (only matching $PO_4^{3-}{}_{(aq)}$ and $Fe_{(s)}$) (Figure 19, 24, and 27). The $Fe_{(aq)}/PO_4^{3-}{}_{(aq)}$ ratio indicates favorable conditions for P trapping below 5 cm exclusively for TN-P (Figure 20). TN-M observes $Fe_{(aq)}/PO_4^{3-}{}_{(aq)}$ ratios <3 throughout the core (Figure 20). An increase in $Fe_{(s)}$ is not observed in TN which indicates that additions were not high enough to push the lake system towards long-term ferrous wheel cycling. However, a noticeable increase in $P_{(s)}$ towards the surface is recorded suggesting that increased trapping has occurred (Figure 24). Due to the lakes low surface water $SO_4^{2-}{}_{(aq)}$ concentrations and constant OM content with depth, $S^{2-}{}_{(aq)}$ is interpreted to be limited in the sediments (Figure 19 and 24). In view of minor expected $S^{2-}{}_{(aq)}$ presence, it is possible that minor quantities of vivianite have been precipitated. Increasing $Fe(II)_{(aq)}$ and $PO_4^{3-}{}_{(aq)}$ concentrations coupled to the $Fe_{(aq)}/PO_4^{3-}{}_{(aq)}$ ratio suggests highly favorable conditions for vivianite (ratio of 3 Fe/2 P) between ~5 cm and 17 cm, which results in a slightly oversaturated index for vivianite (Figure 16 and 19-20). Due to low $Fe_{(aq)}/PO_4^{3-}{}_{(aq)}$ ratios in the upper sediments, I conclude that the TN ferrous wheel is not operating, but that vivianite presence is likely as a result of low surface water $SO_4^{2-}{}_{(aq)}$.

5.4 Aqueous Fe(III)

$Fe(III)_{(aq)}$ is present in the cores of several treated lakes (Figure 17, 19, and 21). This could be due to oxygen introduced during sampling and analysis. However, this may also be due to the presence of dissolved organic carbon ligands increasing Fe(III) solubility (Sholkovitz and Copland, 1981; Schwertmann, 1991). Additionally, the presence of organic ligands may push the redox coupling of $Fe(III)_{(s)}$/Fe(II) below the $SO_4^{2-}{}_{(aq)}$ reduction zone (Stumm and Morgan, 1996). Similarly, the rate of

organotrophic iron reduction of ferrihydrite has been decreased due to surface site $PO_4^{3-}{}_{(aq)}$ adsorption (Borch et al. 2007) Therefore, the $Fe(III)_{(aq)}$ concentrations presented in figures 17, 19, and 21 are being interpreted as a component of the Fe dynamics occurring in shallow lakes ultimately driven by iron addition treatments.

The $Fe(III)_{(aq)}$ presence is not uniform across all treated cores and is likely influenced by substrate type (controlling Fe fluxes) and nutrient loading. The depth of $Fe(III)_{(aq)}$ in TN-M and TN-P are suggested to be results of upper sediment layer redox zonation processes in which the TN-M redox zone is closer to the SWI (Figure 4 and 19). In SL recent additions have resulted in high concentrations of $Fe(III)_{(aq)}$ (and $Fe(II)_{(aq)}$). There is strong overlap of SL $Fe(III)_{(aq)}$ between cores, although, TN-M $Fe(II)_{(aq)}$ presence appears to be hindered by $Fe(II)_{(aq)}$ reducibility or groundwater transport (Figure 7 and 17). BM $Fe(III)_{(aq)}$ is proposed to be driven by a recent influx of iron working in a similar process to that of SL-P (Figure 21). NW-P $Fe(III)_{(aq)}$ presence is likely due to the ~25 years since treatment and organic ligand iron complexation resulting in eventual solubility of iron oxides and $Fe(III)_{(aq)}$ appearance towards the core terminus (Sholkovitz and Copland, 1981; Schwertmann, 1991). Differences in the NW substrates indicates inhibited effect of $Fe_{(aq)}$ treatments on $Fe_{(s)}$ mineral storage in sandy substrates (Figure 25).

5.5 Iron addition for P fixation

Iron has been added to lakes SL, GV, TN, and NW to bind P. Iron binds P adsorbed to the surface of $Fe(III)_{(s)}$ in oxic zones at a 0.6* P:Fe ratio or as mineralized vivianite in anoxic zones at a P:Fe ratio of 0.7 (* for oxidized groundwater; van der Grift et al., 2016; Stumm and Morgan, 1996). The duration of P binding is driven by its form and redox reactivity (Table 1 – 2, Figure 2). The form of P is driven by dissolved oxygen concentration and redox zonation processes (Figure 6). The combined processes control the quantity of P stored in the sediments.

In all treatment lakes, iron addition has led to an increased sedimentary P contribution (Figure 23-25). This is likely due to Fe locking P adsorbed to iron oxides or mineralized as vivianite. Direct proof of vivianite or iron oxides has not been shown, but its presence has been suggested (above) based on water and sediment analysis (Figure 17-25). Based on the similarities between the $Fe_{(s)}$ and $P_{(s)}$ sediment profiles it can be inferred that Fe treatment is contributing to the upper core $P_{(s)}$ increase (Figure 23-25). P bound to reactive iron is proposed to be elevating the upper sediment $P_{(s)}$ fraction in lake SL, GV*, and NW compared to their core terminus concentrations (GV behaves differently due to a sediment injection treatment method and duration since treatment). The quantity is not calculated here but is visually significant and responsible for some phosphate binding (Figure 23-25). This corresponds with lake manger reported reduced surface $PO_4^{3-}{}_{(aq)}$ and less eutrophic conditions over certain time periods. Additionally, water profiles and calculated indices show a likelihood that $PO_4^{3-}{}_{(aq)}$ has also been bound as hematite, vivianite or calcium phosphate minerals fluorapatite and hydroxyapatite (Figure 16, 17, 19, 21). Similarly, the $Fe_{(s)}$ and $P_{(s)}$ profiles indicate that downcore P has also been influenced by iron addition in NW, SL-P, and GV (Figure 23-25). This has likely occurred when reactive iron and P mineralize as authigenic vivianite.

$SO_4^{2-}{}_{(aq)}$ is known to impede vivianite formation (Rothe et al., 2015). In the treated lakes high surface $SO_4^{2-}{}_{(aq)}$ contributes to $S^{2-}{}_{(aq)}$ production throughout most of the cores. This results in FeS_x formation where vivianite would otherwise be more favored, although once $S^{2-}{}_{(aq)}$ is removed vivianite may mineralize.

5.6 Continued research

Field and laboratory work recommendations are provided in appendix 5. Continued research should focus on qualifying Fe and P in NW-P and SL. NW-P and SL represent ~20 years treatment difference and both have high surface water $SO_4^{2-}{}_{(aq)}$ indicating that qualification would provide a timeline of mineralization processes. TN $Fe_{(s)}$ qualification should be investigated as a source for $Fe(III)_{(aq)}$ controlling factors. $Fe(III)_{(aq)}$ presence should also be investigated through anoxic methods. Fe(III) mineral ratios should be investigated at the towards the SWI and downcore for presence of reactive iron and P:Fe ratios for the respective size fractions. In addition, experiments should be conducted on the long-term binding capacity of $FeCl_3$ addition followed by a sand covering layer applied at a later date.

5. Conclusion

Eutrophication is the leading problem facing freshwaters in the current and coming decade. The role of iron addition in long-term phosphate binding for eutrophication remediation has been investigated. Fieldwork analysis has revealed surface water parameters while laboratory-based surface and porewater analysis has determined elemental composition. $Fe(II)_{(aq)}$, $Fe(III)_{(aq)}$, $PO_4^{3-}{}_{(aq)}$, and NH_4^+ has been evaluated spectrophometrically then compared to total concentrations and ligands by ICP-OES and IC analysis. Sediment layers were sliced in an anoxic environment then freeze-dried before analysis by CN, CS, TGA, and XRF-P to determine sediment composition.

Catchment history and nutrient loading play an important role in P trapping (Orihel et al., 2017). Results indicate high treatment iron recovery and increased sedimentary P fixation. The high concentration of iron in the treated lake sediments and porewater are directly related to iron addition. Nevertheless, recovery percentages were lower in wind distributed iron treatments indicating that surface microcurrents may influence iron deposit zones. This would promote zones of increased iron storage and zones where P may be internally loaded. This may be indicated in SL where a heterogeneous sediment recovery was recorded. Although SL's recovery may also be a result of groundwater flux. Within the treated lakes groundwater levels overlap the lake areas and flows would likely remove dissolved and colloidal particles from the lake area.

Within the sampled shallow lake environments, distinct redox zonation based on overall energy-yielding redox reactions is not present. However, redox zonation in treated lakes has been affected by iron addition. Elevated $Fe(III)_{(aq)}$ and $Fe(II)_{(aq)}$ concentrations at deeper depths have indicated that iron reduction is occurring over a larger depth interval. This has resulted in the simultaneous reduction zonation of both Fe and $SO_4^{2-}{}_{(aq)}$ and ultimately indicates an effect on iron redox cycling and a perceived effect on authigenic vivianite formation. This $Fe(II)_{(aq)}$ effect is would be due to the increased depth over which $Fe(II)_{(aq)}$ is present thus increasing the likelihood that $S^{2-}{}_{(aq)}$ is absent (by gaseous escape), removing a limitation on authigenic vivianite mineralization. Without $S^{2-}{}_{(aq)}$ gaseous escape authigenic vivianite mineralization will not occur at deeper depths due to favorable FeS_x mineralization. If $S^{2-}{}_{(aq)}$ is present, $Fe(II)_{(aq)}$ will not diffuse upwards. As the ferrous wheel is controlled by redox processes, OM content, and surface water $SO_4^{2-}{}_{(aq)}$ concentration. $S^{2-}{}_{(aq)}$ production and iron sulfide formation (FeS_x) is likely to limit iron mobility and limit upward diffusing $Fe(II)_{(aq)}$ for oxidation and subsequent $PO_4^{3-}{}_{(aq)}$ binding to the oxic zone (Kleeberg et al., 2012).

The unexpected presence of Fe^{3+} in all treated lakes and BM represents conditions in which ferric iron additions cannot be fully reduced or that microbial iron reduction is rate limited. Two mechanisms for

Fe^{3+} presence are proposed. First, high surface P binding on filterable iron (oxy-)hydroxides is presented as a factor limiting microbial ability to reduce Fe^{3+}. Secondly, reactive iron complexation with organic ligands could have restricted the reducibility of reactive iron until it is more energetically favored deeper in the sediments. I propose further research into Fe^{3+} presence through speciation investigations targeting the binding rate of upper and lower core $Fe_{(s)}$ fractions. This should be coupled to microbe and organic ligand analysis.

Despite some lakes being from the same lake complex, all lakes did have their own characteristics which are likely related to use history, management procedure, and physical processes/properties. Additionally, differences exist between core locations. The specific effects of iron addition on redox zonation within these lake systems is not universally similar. These lake characteristics appear to influence processes that will ultimately affect the fate of solid phase Fe and P in the sediments and ultimately complicating generalizations. However, all lakes have showed signs of an fortified ferrous wheel has likely increased FeS_x and authigenic vivianite mineralization leading to increased PO_4^{3-} fixation. Overall, iron addition for long-term phosphate fixation is suggested as viable in treated lakes. Specific treatment methods and quantities must be determined for each lake as microcurrents, surface $SO_4^{2-}{}_{(aq)}$, and groundwater flows which are indicated as affected long-term P fixation.

References

Anderson, D.M. and Garrison, D.J. eds., 1997. The ecology and oceanography of harmful algal blooms. American Society of Limnology and Oceanography.

Berner, R.A., 1970. Sedimentary pyrite formation. American journal of science, 268(1), pp.1-23.

Berner, R.A., 1981. A new geochemical classification of sedimentary environments. Journal of Sedimentary Research, 51(2), pp.359-365.

Boers, P.C.M., 1991. The release of dissolved phosphorus from lake sediments (Doctoral dissertation, Boers).

Borch, T., Masue, Y., Kukkadapu, R.K. and Fendorf, S., 2007. Phosphate imposed limitations on biological reduction and alteration of ferrihydrite. Environmental science & technology, 41(1), pp.166-172.

Brouwer Group, 1993. Hydrografische gegevens van meren en plassen. Projectnummer: 080912.

Burdige, D.J. (2011). 5.09 - Estuarine and Coastal Sediments – Coupled Biogeochemical Cycling, Treatise on Estuarine and Coastal Science, 279-316, ISBN 9780080878850, Academic Press. https://doi.org/10.1016/B978-0-12-374711-2.00511-8.

Burdige, D.J., 2006. Geochemistry of marine sediments. Princeton University Press.

Burley, K.L., Prepas, E.E. and Chambers, P.A., 2001. Phosphorus release from sediments in hardwater eutrophic lakes: the effects of redox-sensitive and-insensitive chemical treatments. Freshwater Biology, 46(8), pp.1061-1074.

B-ware Sloene (2018). Beijzering Sloene: Kwaliteit van het oppervlaktewater, waterbodem en bodemvocht in 2017 Rapportage Opdrachtgever: Hoogheemraadschap van Rijnland • Projectnummer PR-13.063d Rapportnummer 13.063D.. Rapportnummer 13.063D.17.100a. Nijmegen, pp.9-47. (In Dutch)

B-ware Sloene (2018). Beijzering Sloene: Kwaliteit van het oppervlaktewater, waterbodem en bodemvocht in 2017 Rapportage Opdrachtgever: Hoogheemraadschap van Rijnland • Projectnummer PR-13.063d Rapportnummer 13.063D.. Rapportnummer 13.063D.17.100a. Nijmegen, pp.9-47. (In Dutch)

Cai, W.J. and Sayles, F.L., 1996. Oxygen penetration depths and fluxes in marine sediments. Marine Chemistry, 52(2), pp.123-131.

Carpenter, S.R., Caraco, N.F., Correll, D.L., Howarth, R.W., Sharpley, A.N. and Smith, V.H., 1998. Nonpoint pollution of surface waters with phosphorus and nitrogen. Ecological applications, 8(3), pp.559-568.

Chrzanowski, C., Geurts, J.J.M., Heerdt, G.T. and Declerck, S., 2015. Praktijkproef ijzersuppletie voor fosfaatvastlegging in laagveenplassen.

Cooke, G.D., Welch, E.B., Martin, A.B., Fulmer, D.G., Hyde, J.B. and Schrieve, G.D., 1993. Effectiveness of Al, Ca, and Fe salts for control of internal phosphorus loading in shallow and deep lakes. Hydrobiologia, 253(1-3), pp.323-335.

Cooke, G.D., Welch, E.B., Peterson, S. and Nichols, S.A., 2016. Restoration and management of lakes and reservoirs. CRC press.

Copetti, D., Finsterle, K., Marziali, L., Stefani, F., Tartari, G., Douglas, G., Reitzel, K., Spears, B.M., Winfield, I.J., Crosa, G. and d'Haese, P., 2016. Eutrophication management in surface waters using lanthanum modified bentonite: a review. Water research, 97, pp.162-174.

Cornell, R.M. and Schwertmann, U., 2003. The iron oxides: structure, properties, reactions, occurrences and uses. John Wiley & Sons.

Curtis, C.D., Coleman, M.L. and Love, L.G., 1986. Pore water evolution during sediment burial from isotopic and mineral chemistry of calcite, dolomite and siderite concretions. Geochimica et Cosmochimica Acta, 50(10), pp.2321-2334.

Davison, W., 1985. Conceptual models for transport at a redox boundary. Chemical Processes in Lakes, John Wiley and Sons, New York New York. 1985. p 31-53, 9 fig, 59 ref.

Deppe, T. and Benndorf, J., 2002. Phosphorus reduction in a shallow hypereutrophic reservoir by in-lake dosage of ferrous iron. Water Research, 36(18), pp.4525-4534.

Dodds, W.K., Bouska, W.W., Eitzmann, J.L., Pilger, T.J., Pitts, K.L., Riley, A.J., Schloesser, J.T. and Thornbrugh, D.J., 2008. Eutrophication of US freshwaters: analysis of potential economic damages.

Downing, J.A., 2014. Limnology and oceanography: two estranged twins reuniting by global change. Inland Waters, 4(2), pp.215-232.

Ekholm, P. and Lehtoranta, J., 2012. Does control of soil erosion inhibit aquatic eutrophication?. Journal of environmental management, 93(1), pp.140-146.

Frank, Tableau Public. 2019. Beijzering sloene. [ONLINE] Available at: https://public.tableau.com/profile/frank2554#!/vizhome/sloenen/Beijzeringsloene. [Accessed 2 April 2019].

Froelich, P.N., Klinkhammer, G.P., Bender, M.L., Luedtke, N.A., Heath, G.R., Cullen, D., Dauphin, P., Hammond, D., Hartman, B., Maynard, V., (1979). Early oxidation of organic matter in pelagic sediments of the eastern equatorial Atlantic: suboxic diagenesis. Geochimica et Cosmochimica Acta 43, 1075–1090.

Gächter, R. and Müller, B., 2003. Why the phosphorus retention of lakes does not necessarily depend on the oxygen supply to their sediment surface. Limnology and Oceanography, 48(2), pp.929-933.

Geurts, J.J., Smolders, A.J., Verhoeven, J.T., Roelofs, J.G. and Lamers, L.P., 2008. Sediment Fe: PO4 ratio as a diagnostic and prognostic tool for the restoration of macrophyte biodiversity in fen waters. Freshwater Biology, 53(10), pp.2101-2116.

Ghiorse, W.C., 1984. Biology of iron-and manganese-depositing bacteria. Annual review of microbiology, 38(1), pp.515-550.

Gulati, R.D. and Van Donk, E., 2002. Lakes in the Netherlands, their origin, eutrophication and restoration: state-of-the-art review. In Ecological Restoration of Aquatic and Semi-Aquatic Ecosystems in the Netherlands (NW Europe)(pp. 73-106). Springer, Dordrecht.

Gunnars, A., Blomqvist, S., Johansson, P. and Andersson, C., 2002. Formation of Fe (III) oxyhydroxide colloids in freshwater and brackish seawater, with incorporation of phosphate and calcium. Geochimica et Cosmochimica Acta, 66(5), pp.745-758.

Hall, R.I. and Smol, J.P., 1999. Diatoms as indicators of lake eutrophication. The diatoms: applications for the environmental and earth sciences, pp.128-168.

Hansen, J., Reitzel, K., Jensen, H.S. and Andersen, F.Ø., 2003. Effects of aluminum, iron, oxygen and nitrate additions on phosphorus release from the sediment of a Danish softwater lake. Hydrobiologia, 492(1-3), pp.139-149.

Hoeksema, R.J., 2007. Three stages in the history of land reclamation in the Netherlands. Irrigation and Drainage: The journal of the International Commission on Irrigation and Drainage, 56(S1), pp.S113-S126. (In Dutch)

House, W.A. and Denison, F.H., 2000. Factors influencing the measurement of equilibrium phosphate concentrations in river sediments. Water Research, 34(4), pp.1187-1200.

Hupfer, M. and Lewandowski, J., 2008. Oxygen controls the phosphorus release from lake sediments–a long-lasting paradigm in limnology. International Review of Hydrobiology, 93(4-5), pp.415-432.

Hutchinson, G.E., 1957. A Treatise on Limnology, 1, p.243.

Inskeep, W.P. and Silvertooth, J.C., 1988. Inhibition of hydroxyapatite precipitation in the presence of fulvic, humic, and tannic acids. Soil Science Society of America Journal, 52(4), pp.941-946.

Inskeep, W.P. and Silvertooth, J.C., 1988. Kinetics of hydroxyapatite precipitation at pH 7.4 to 8.4. Geochimica et Cosmochimica Acta, 52(7), pp.1883-1893.

Ionescu, D., Heim, C., Polerecky, L., Thiel, V. and De Beer, D., 2015. Biotic and abiotic oxidation and reduction of iron at circumneutral pH are inseparable processes under natural conditions. Geomicrobiology Journal, 32(3-4), pp.221-230.

Jaeger, D., 1994. Effects of hypolimnetic water aeration and iron-phosphate precipitation on the trophic level of Lake Krupunder. Hydrobiologia, 275(1), pp.433-444.

Jones, C.A. and Welch, E.B., 1990. Internal phosphorus loading related to mixing and dilution in a dendritic, shallow prairie lake. Research Journal of the Water Pollution Control Federation, pp.847-852.

Jørgensen, B.B. and Kasten, S., 2006. Sulfur cycling and methane oxidation. In Marine geochemistry (pp. 271-309). Springer, Berlin, Heidelberg.

Kirk, G.J.D., Yu, T.R. and Choudhury, F.A., 1990. Phosphorus chemistry in relation to water regime. In Phosphorus requirements for sustainable agriculture in Asia and Oceania. Proceedings of a symposium, 6-10 March 1989. (pp. 211-223). International Rice Research Institute.

Kleeberg, A., Herzog, C. and Hupfer, M., 2013. Redox sensitivity of iron in phosphorus binding does not impede lake restoration. Water research, 47(3), pp.1491-1502.

Kleeberg, A., Köhler, A. and Hupfer, M., 2012. How effectively does a single or continuous iron supply affect the phosphorus budget of aerated lakes?. Journal of soils and sediments, 12(10), pp.1593-1603.

Lehtoranta, J. and Heiskanen, A.S., 2003. Dissolved iron: phosphate ratio as an indicator of phosphate release to oxic water of the inner and outer coastal Baltic Sea. Hydrobiologia, 492(1-3), pp.69-84.

Mettrop, I. IJzersuppletie in laagveenplassen: een mitigerende maatregel ter vervanging van verdwenen ijzerrijke kwel. Een verslag van de pilot. Amsterdam: Universiteit van Amsterdam; 2009. (In Dutch)

NIST, 2004 National Institute of Standards and Technology database version 8 NIST X-ray Photoelectron Spectroscopy Database, Version 3.5.

Nriagu, J.O., 1972. Stability of vivianite and ion-pair formation in the system fe3 (PO4) 2-H3PO4H3PO4-H2o. Geochimica et Cosmochimica Acta, 36(4), pp.459-470.

Orihel, D.M., Baulch, H.M., Casson, N.J., North, R.L., Parsons, C.T., Seckar, D.C. and Venkiteswaran, J.J., 2017. Internal phosphorus loading in Canadian fresh waters: a critical review and data analysis. Canadian Journal of Fisheries and Aquatic Sciences, 74(12), pp.2005-2029.

Personal communication Bart Schaub Hoogheemraadschap Rijnland

Personal communication Gerard Ter Heerdt, Waternet

Postma, D. and Jakobsen, R., 1996. Redox zonation: equilibrium constraints on the Fe (III)/SO4-reduction interface. Geochimica et Cosmochimica Acta, 60(17), pp.3169-3175.

Postma, D., 1981. Formation of siderite and vivianite and the pore-water composition of a recent bog sediment in Denmark. Chemical Geology, 31, pp.225-244.Berner, 1981b

Quaak, M., van der Does, J., Boers, P. and van der Vlugt, J., 1993. A new technique to reduce internal phosphorus loading by in-lake phosphate fixation in shallow lakes. Hydrobiologia, 253(1-3), pp.337-344.

Raiswell, R. and Canfield, D.E., 2012. The iron biogeochemical cycle past and present. Geochemical perspectives, 1(1), pp.1-2.

Rothe, M., Kleeberg, A., Grüneberg, B., Friese, K., Pérez-Mayo, M. and Hupfer, M., 2015. Sedimentary sulphur: iron ratio indicates vivianite occurrence: a study from two contrasting freshwater systems. Plos one, 10(11), p.e0143737.

Schindler, D.W., 2006. Recent advances in the understanding and management of eutrophication. Limnology and oceanography, 51(part2), pp.356-363.

Schindler, D.W., 2012. The dilemma of controlling cultural eutrophication of lakes. Proc. R. Soc. B, p.rspb20121032.

Schlesinger, W.H. and Bernhardt, E.S., 2013. Biogeochemistry: an analysis of global change. Academic press.

Schwertmann, U., 1991. Solubility and dissolution of iron oxides. Plant and soil, 130(1-2), pp.1-25.

Sholkovitz, E.R. and Copland, D., 1981. The coagulation, solubility and adsorption properties of Fe, Mn, Cu, Ni, Cd, Co and humic acids in a river water. Geochimica et Cosmochimica Acta, 45(2), pp.181-189.

Sholkovitz, E.R. and Copland, D., 1981. The coagulation, solubility and adsorption properties of Fe, Mn, Cu, Ni, Cd, Co and humic acids in a river water. Geochimica et Cosmochimica Acta, 45(2), pp.181-189.

Sholkovitz, E.R. and Copland, D., 1981. The coagulation, solubility and adsorption properties of Fe, Mn, Cu, Ni, Cd, Co and humic acids in a river water. Geochimica et Cosmochimica Acta, 45(2), pp.181-189.

Shortle, J.S. and Horan, R.D., 2001. The economics of nonpoint pollution control. Journal of economic surveys, 15(3), pp.255-289.

Smith, L., Watzin, M.C. and Druschel, G., 2011. Relating sediment phosphorus mobility to seasonal and diel redox fluctuations at the sediment–water interface in a eutrophic freshwater lake. Limnology and Oceanography, 56(6), pp.2251-2264.

Smith, V.H., Tilman, G.D. and Nekola, J.C., 1999. Eutrophication: impacts of excess nutrient inputs on freshwater, marine, and terrestrial ecosystems. Environmental pollution, 100(1-3), pp.179-196.

Smolders AJP & Roelofs JGM (1993) Sulphate-mediated iron limitation and eutrophication in aquatic ecosystems. Aquat. Bot. 46: 247–253

Smolders, A.J.P., Lamers, L.P.M., Moonen, M., Zwaga, K. and Roelofs, J.G.M., 2001. Controlling phosphate release from phosphate-enriched sediments by adding various iron compounds. Biogeochemistry, 54(2), pp.219-228.

Stigebrandt, A., Rahm, L., Viktorsson, L., Ödalen, M., Hall, P.O. and Liljebladh, B., 2014. A new phosphorus paradigm for the Baltic proper. Ambio, 43(5), pp.634-643.

Straub, K.L., Benz, M. and Schink, B., 2001. Iron metabolism in anoxic environments at near neutral pH. FEMS microbiology ecology, 34(3), pp.181-186.

Straub, K.L., Benz, M., Schink, B. and Widdel, F., 1996. Anaerobic, nitrate-dependent microbial oxidation of ferrous iron. Appl. Environ. Microbiol., 62(4), pp.1458-1460.

Stumm, W. and Morgan, J.J., 1996. Aquatic Chemistry: Chemical Equilibria and Rates in Natural Waters {Environmental Science and Technology}. Wiley.

Ter Heerdt, G., Geurts, J., Immers, A., Colin, M., Olijhoek, P., Yedema, E., Baars, E. and Voort, J.W., 2012. Ijzersuppletie in laagveenplassen: De resultaten.

Torenbeek, R., 2013. Gebiedsdocument Reeuwijkse Plassen: Mogelijke maatregelen voor verbetering van de ecologische kwaliteit. Hoogheemraadschap van Rijnland. (In Dutch)

van der Grift, B., Behrends, T., Osté, L.A., Schot, P.P., Wassen, M.J. and Griffioen, J., 2016. Fe hydroxyphosphate precipitation and Fe (II) oxidation kinetics upon aeration of Fe (II) and phosphate-containing synthetic and natural solutions. Geochimica et Cosmochimica Acta, 186, pp.71-90.

van der Grift, B., Rozemeijer, J.C., Griffioen, J. and van der Velde, Y., 2014. Iron oxidation kinetics and phosphate immobilization along the flow-path from groundwater into surface water. Hydrology and Earth System Sciences, 18(11), pp.4687-4702.

Van Liere, L., 1986. Loosdrecht Lakes, origin, eutrophication, restoration and research programme. Hydrobiological Bulletin, 20(1-2), pp.9-15.

Veeningen, R., 1996. Restoration of the Lake Nannewijd: First Results (tech.), Restoration of the Lake Nannewijd: First Results. Water Authority Friesland, Leeuwarden.

Verweij, W., 2005. CHEAQS PRO: A program for calculating chemical equilibria in aquatic systems. RIVM, Bilthoven, Version, 2005.

Wang, J., Chen, J., Guo, J., Sun, Q. and Yang, H., 2018. Combined Fe/P and Fe/S ratios as a practicable index for estimating the release potential of internal-P in freshwater sediment. Environmental Science and Pollution Research, 25(11), pp.10740-10751.

Waterschap Friesland (1995). Evaluatie fosfaatfixatie Nannewijd. Leeuwarden 1995. (In Dutch)

Witteveen & Bos (2012). Evaluatie van het KRW-project flexibel peilbeheer Fryslân bijlagenrapport. Projectnummer LW307-1 Referentie LW307-1/strg/004 Deventer, pp. 9-120. (In Dutch)

Wolter, K.D., 2010. Restoration of eutrophic lakes by phosphorus precipitation, with a case study on Lake Gross-Glienicker. In Restoration of Lakes, Streams, Floodplains, and Bogs in Europe (pp. 85-99). Springer, Dordrecht.

Appendix 1: Iron oxides

Table 1: The 16 iron oxides. From Cornell and Schertmann, 2003

Oxide–hydroxides and hydroxides	***Oxides***
Goethite α-FeOOH	Hematite α-Fe_2O_3
Lepidocrocite γ-FeOOH	Magnetite Fe_3O_4 ($Fe^{II}Fe^{III}_2O_4$)
Akaganéite β-FeOOH	Maghemite γ-Fe_2O_3
Schwertmannite $Fe_{16}O_{16}(OH)_y(SO_4)_z \cdot n\ H_2O$	β-Fe_2O_3
δ-FeOOH	ε-Fe_2O_3
Feroxyhyte δ′-FeOOH	Wüstite FeO
High pressure FeOOH	
Ferrihydrite $Fe_5HO_8 \cdot 4\ H_2O$	
Bernalite $Fe(OH)_3$	
$Fe(OH)_2$	
Green Rusts $Fe^{III}_xFe^{II}_y(OH)_{3x+2y-z}(A^-)_z$; $A^- = Cl^-$; ½ SO_4^{2-}	

Appendix 2: $Fe(II)_{(s)}Fe(III)_{(s)}$ minerals

Recently, vivianite has been described as a final product of the “green rust” mineral fougèrite which is found in waterlogged clay containing soils and sediments (Mills et al., 2012). Laboratory studies have shown that in the presence of high PO_4^{3-} concentrations vivianite and green rust formation is a result of nitrate reducing, iron oxidizing bacteria as well as dissimilatory iron-reducing bacteria (DIRB) (Miot et al., 2009; Barthélémy et al., 2012; O’Loughlin et al., 2013; Etique et al., 2014). Green rusts are metastable and their ligand replacement determines the terminal mineral form (Mills et al., 2012). It is therefore proposed that in high iron dosage treated lake sediments that green rusts may form and add further redox control mechanisms to PO_4^{3-} fixation treatments.

Appendix 3: Data files

All data files will be provided separately as Microsoft Excel documents.

Final data

Data treatment (Sediments, porewaters, calculations)

Raw Data

Notes

Appendix 4: Surface water parameters

Table 2: Surface water EC, pH, dissolved oxygen, temperature, and secchi disk depth. Secchi disk was visible at the lake bed for both cores from Terra Nova. Lake Vuntus's middle core had little sediment and was mainly hard peat. Nannewijd's middle core

Sample ID	EC (µS/cm)	pH	Dissolved O2 (mg/L)	Temperature (°C)	Secchi disk depth (m)
SL-P	481	7.52	7.86	8.7	1.8
SL-M	480	7.72	7.86	8.75	1.85
GV-P	469	8.01	11.53	9.4	0.5
GV-M	468	8.05	11.2	9.35	0.4
GK-P	507	8.07	11.14	9.3	0.4
GK-M	506	8.05	11.05	9.4	0.5
TN-P	343	6.78	11.07	3.85	1.65
TN-M	330	7.45	11.01	3.8	1.05
VT-P	400	8	12.11	4	1
VT-M	393	7.97	12.17	4	0.9
NW-P	574	8.46	12.12	5.1	1.05
NW-M	591	8.51	12.14	4.95	1.16
BM-P	713	8.25	11.82	4.2	0.4
BM-M	747	8.25	12.06	4.35	0.45

Appendix 5: Continued field and laboratory work

The use of rhizons provides a potential source of oxygen entry and contamination to core sampling. Therefore, it is suggested that porewater sampling be done in an anoxic environment. Desiccation of sediments should be done first through centrifugation followed by freeze-drying.